UC Davis
UC Davis Previously Published Works

Title

Single-nucleus Atlas of Sevoflurane-induced Hippocampal Cell Type– and Sex-specific
Effects during Development in Mice

Permalink

Journal

ISSN

Authors

Song, Shao-yong
Peng, Ke
Meng, Xiao-wen
et al.

Publication Date

DOI

Copyright Information

Peer reviewed

ANESTHESIOLOGY

Single-nucleus Atlas of Sevoflurane-induced Hippocampal Cell Type– and Sex-specific Effects during Development in Mice

Shao-yong Song, M.D., Ph.D., Ke Peng, M.D., Ph.D., Xiao-wen Meng, Ph.D., Xi-sheng Shan, M.D., Ph.D., Qing-cai Chen, M.D., Wei-ming Zhao, M.D., Biyu Shen, M.D., Hong Qiu, Ph.D., Hong Liu, M.D., FASE, Hua-yue Liu, M.D., Fu-hai Ji, M.D., Ph.D.

ANESTHESIOLOGY 2023; 138:477–96

EDITOR'S PERSPECTIVE

What We Already Know about This Topic

- Multiple neonatal exposures to sevoflurane induce neurocognitive dysfunction in rodents
- The cell type–specific mechanisms underlying these cognitive deficits are incompletely understood

What This Article Tells Us That Is New

- Single-nucleus RNA sequencing revealed cell type– and sex-specific effects of repeated sevoflurane exposure in the hippocampus of neonatal mice
- These differential effects of sevoflurane on distinct hippocampal cell populations and signaling pathways provide new insights into the mechanisms of actions of anesthetics in the developing brain

ABSTRACT

Background: Multiple neonatal exposures to sevoflurane induce neurocognitive dysfunctions in rodents. The lack of cell type–specific information after sevoflurane exposure limits the mechanistic understanding of these effects. In this study, the authors tested the hypothesis that sevoflurane exposures alter the atlas of hippocampal cell clusters and have neuronal and nonneuronal cell type–specific effects in mice of both sexes.

Methods: Neonatal mice were exposed to 3% sevoflurane for 2 h at postnatal days 6, 8, and 10 and analyzed for the exposure effects at postnatal day 37. Single-nucleus RNA sequencing was performed in the hippocampus followed by *in situ* hybridization to validate the results of RNA sequencing. The Morris Water Maze test was performed to test neurocognitive function.

Results: The authors found sex-specific distribution of hippocampal cell types in control mice alongside cell type– and sex-specific effects of sevoflurane exposure on distinct hippocampal cell populations. There were important changes in male but not in female mice after sevoflurane exposure regarding the proportions of cornu ammonis 1 neurons (control *vs.* sevoflurane, males: 79.9% *vs.* 32.3%; females: 27.3% *vs.* 24.3%), dentate gyrus (males: 4.2% *vs.* 23.4%; females: 36.2% *vs.* 35.8%), and oligodendrocytes (males: 0.6% *vs.* 6.9%; females: 5.9% *vs.* 7.8%). In male but not in female mice, sevoflurane altered the number of significantly enriched ligand–receptor pairs in the cornu ammonis 1, cornu ammonis 3, and dente gyrus trisynaptic circuit (control *vs.* sevoflurane, cornu ammonis 1–cornu ammonis 3: 18 *vs.* 42 in males and 15 *vs.* 21 in females; cornu ammonis 1–dentate gyrus: 21 *vs.* 35 in males and 12 *vs.* 20 in females; cornu ammonis 3–dentate gyrus: 25 *vs.* 45 in males and 17 *vs.* 20 in females), interfered with dentate gyrus granule cell neurogenesis, hampered microglia differentiation, and decreased cornu ammonis 1 pyramidal cell diversity. Oligodendrocyte differentiation was specifically altered in females with increased expressions of *Mbp* and *Mag*. *In situ* hybridization validated the increased expression of common differentially expressed genes.

Conclusions: This single-nucleus RNA sequencing study reveals the hippocampal atlas of mice, providing a comprehensive resource for the neuronal and nonneuronal cell type– and sex-specific effects of sevoflurane during development.

(*ANESTHESIOLOGY* 2023; 138:477–96)

<zdoi;10.1097/ALN.0000000000004522>

The neonatal and early childhood period is a critical developmental window of vulnerability to cognitive disorders.[1] During this period, multiple exposures to anesthetics are reported to affect brain development in rodents and nonhuman primates.[2] In addition, sex-specific differences exist in the timeline of brain development.[3] It has been shown that anesthetic exposure at postnatal day 7 caused cognitive impairment in male but not female rats.[4] Thus, anesthetic susceptibility may differ between the sexes during neonatal anesthetic exposures.

Sevoflurane is the most widely used anesthetic for induction and maintenance of anesthesia in pediatric surgeries. Hippocampal dysfunction induced by neonatal sevoflurane exposures led to memory loss and cognitive impairment.[5,6] The hippocampus is a highly complex interactive structure of pyramidal cells in the cornu ammonis regions (cornu ammonis 1, cornu ammonis 2, and cornu ammonis 3) and dentate gyrus granule cells. Glial cells including astrocytes, microglia, oligodendrocytes, and oligodendrocyte precursor cells underpin the cytoarchitecture and physiologic functions of the hippocampus. Anesthetics may have multiple effects on different hippocampal cell types.[7] Sevoflurane exposures resulted in cognitive deficits, which were associated with decreased differentiation and neurogenesis of dentate gyrus neural progenitors.[7] Sevoflurane has been reported to induce tau trafficking from neurons to activate microglia,[8] compromise astrocyte morphogenesis related to synaptic overgrowth,[9] and disrupt oligodendrocyte maturation and myelination.[10] Our recent study confirmed the behavioral changes and cognitive disorders after multiple neonatal sevoflurane exposures in mice and revealed hippocampal genomic profile using the messenger RNA (mRNA) sequencing.[11] Nevertheless, the analysis of bulk hippocampus may mask the most vulnerable cell types and crucial signaling pathways. To date, the mechanisms underlying the neuronal and nonneuronal cell type–specific effects of sevoflurane during development are poorly defined, and sex as a key biologic variable remains largely underevaluated in this field.

Here we depicted a single-cell atlas of sevoflurane-induced hippocampal cell type–specific effects in mice of both sexes. We performed single-nucleus RNA sequencing, clustering analyses, cellular cross-talk, single-cell trajectory analyses, differentially expressed genes and enrichment analyses, and experimental validation. We hypothesized that (1) neonatal sevoflurane exposures would alter the atlas of hippocampal cell

clusters in young mice (2) with neuronal and nonneuronal cell type–specific effects and that (3) these effects are sex-specific.

Materials and Methods

Mice, Anesthesia, and Treatment

The animal study protocol was approved by the Ethics Committee for Animal Care and Use of Soochow University, Suzhou, China (approval No.: 202007A098). C57BL/6J mice (8 weeks old, 20 to 25 g, drug- or test-naive) were purchased from the Slaccas Laboratory (China). We report this study according to the Animal Research: Reporting In Vivo Experiments (ARRIVE) guidelines.

In this study, we conducted experiments on male and female offspring mice separately. All mice were housed in a specific pathogen-free room (22 to 24°C) with a 12-h light/dark cycle. The offspring mice were sequentially numbered with ear tags. Using an online randomization tool (https://www.randomizer.org/), we randomly allocated the mice to the control or sevoflurane group on postnatal days 6, 8, and 10. Mice received 60% oxygen balanced with nitrogen (control treatment) or 3% sevoflurane in 60% oxygen balanced with nitrogen (sevoflurane treatment) for 2 h from 9:00 to 11:00 AM. This animal model was described previously.[6] The gas concentration was monitored using a gas analyzer (Vamos; Dräger Medical, Germany). The rectal temperature of every mouse was maintained at 36.5 to 37.5°C by adjusting the heating pad temperature.[5] The 3% sevoflurane is a clinically relevant concentration.[12] This model did not induce adverse changes in the blood gas or electrolytes of mice.[11] Mice were treated and assessed in the sequential order. At 9:00 to 11:00 AM on postnatal day 37, mice were decapitated under brief sevoflurane anesthesia (3% sevoflurane for 3 min) for harvesting hippocampus samples.

The allocation details were stored in an opaque sealed envelope. The investigators who perform the behavior tests, single-nucleus RNA sequencing, fluorescence *in situ* hybridization, real-time quantitative polymerase chain reaction, and Western blot were blinded to the group allocation until the completion of final analysis.

Morris Water Maze

The Morris water maze test was performed to confirm the successful establishment of cognitive impairment model in mice.[11] To evaluate spatial learning ability, the mice were trained to reach the platform sequentially for 5 consecutive days in the training phase (9:00 to 11:00 AM on postnatal days 31 to 35), and the escape latency was recorded. To assess memory function, the platform was removed in the testing phase (9:00 to 11:00 AM on postnatal day 36), and the mice were sequentially assessed in 60 s in the Morris water maze. The platform-crossing times, time spent in the platform quadrant, and mean distance from the original platform area were recorded. All behavioral data in the Morris water

Biyu Shen, M.D.: Shanghai Children's Medical Center Affiliated to Shanghai Jiaotong University School of Medicine, Shanghai, China.

Hong Qiu, Ph.D.: DNA Technologies and Expression Analysis Core, Genome and Biomedical Sciences Facility, University of California-Davis, Davis, California.

Hong Liu, M.D., F.A.S.E.: Department of Anesthesiology and Pain Medicine, University of California-Davis Health, Sacramento, California.

Hua-yue Liu, M.D.: Department of Anesthesiology, First Affiliated Hospital of Soochow University, Suzhou, China; Institute of Anesthesiology, Soochow University, Suzhou, China.

Fu-hai Ji, M.D., Ph.D.: Department of Anesthesiology, First Affiliated Hospital of Soochow University, Suzhou, China; Institute of Anesthesiology, Soochow University, Suzhou, China.

maze were recorded automatically on a video-tracking system with the ANY-maze software (Stoelting Co., USA).

Extraction of Hippocampal Nuclei

The hippocampi were rapidly harvested and dissected into 1- to 2-mm³ tissue blocks in ice-cold phosphate buffered saline at 9:00 to 11:00 AM on postnatal day 37. The hippocampal tissues were ground into a nuclei suspension with 500 ml lysis buffer. After resuspension, centrifugation, and filtration, the hippocampal nuclei were extracted. The nuclei were counted using Trypan blue staining.

Single-nucleus RNA Sequencing Using 10 × Genomics

Barcoded single nucleus, Gel Bead-In-Emulsions, and cDNA libraries were generated and processed following the manufacturer's protocol. Data were analyzed using the 10 × Genomics GemCode Technology (10x Genomics, USA) and OmicShare tools. Every transcript in a single cell was uniquely barcoded using a unique molecular identifier. The single-nucleus RNA sequencing analysis was performed on the Illumina NovaSeq 6000 system (Illumina, USA). The raw sequence data are deposited in the Sequence Read Achieve of the National Center of Biotechnology Information (Bethesda, Maryland; https://www.ncbi.nlm.nih.gov/sra) under accession Nos. PRJNA797582 and PRJNA873858.

Data Quality Control

Cell Ranger software (version 6.1) was utilized for quality control. We analyzed gene counts, unique molecular identifier counts, and percentage of mitochondrial genes, and then we aligned the reads to the musculus transcriptome (Ensembl_release98) using the R package Seurat.[13] The criteria for effective cells were as follows: gene counts 500 to 4,000 per cell, unique molecular identifier counts less than 8,000 per cell, and the percentage of mitochondrial genes less than 10%. Low-quality cells were filtered out. We normalized the filtered gene expression using Seurat's *NormalizeData* function, as follows: a gene expression level =

$$\log \left(1 + \frac{\text{unique molecular identif ierA}}{\text{unique molecular identif ierTOTAL}} \times 10000 \right).$$

Clustering Analysis

After data preprocessing, we used the canonical correlation analysis to normalize and filter the gene matrix. For principal component analysis and dimension reduction, we selected genes with average expression values of 0.01 to 3 and dispersion greater than 0.5.[14] The principal components were applied for t-distributed stochastic neighbor embedding on two dimensions using the *RunTSNE* function in the Seurat.[13] Cluster- or subcluster-specific marker genes were defined from our 10x sequencing dataset using a likelihood-ratio test, based on the following criteria: P value ≤ 0.01, $\log_2$(fold change) 0.361 or greater, and the

percentage of cells where the gene is detected in the specific cluster or subcluster 25% or greater (mincell_pct 0.25 or greater).[15] To resolve the identities of the clusters, canonical cell type–specific markers for major hippocampal neurons and nonneuron cell types were retrieved from previous studies.[16–19] Major hippocampal cell clusters were identified by mapping canonical marker genes on the two-dimensional t-distributed stochastic neighbor embedding map.

In addition, we analyzed functional cell subcluster (such as dentate gyrus granule cells, microglia, and cornu ammonis 1 pyramidal neurons) to discover compositional and transcriptional differences for each subcluster between the control and sevoflurane groups. We performed principal component analysis to identify significant principal components for subsequent clustering and t-distributed stochastic neighbor embedding visualization. We identified subclusters using the Seurat's *FindClusters* function. We utilized the Seurat's *FindAllMarkers* function to confirm differentially expressed genes and specific marker genes for each subcluster.

Cellular Cross-talk Analysis

We used the CellPhoneDB software (version 2.0; https://www.cellphonedb.org)[20] to analyze the expression abundance of ligand–receptor interactions among hippocampal cell types. To be included in the cross-talk analysis, the ligands or receptors should be expressed by 30% or greater cells in a specific cluster (mincell_pct 0.30 or greater). We used the permutation test by randomly distributing the cluster labels of all cells 1,000 times and analyzed the average expression of each ligand–receptor pair between two clusters. We defined P value <0.05 as significant ligand–receptor enrichment. To illustrate the regulation relationship between cell types, we constructed a cell–cell interaction network diagram, with boxes representing the interactions from ligands (source cells) to receptors (target cells).

Single-cell Trajectory Analysis

We constructed single-cell development and differentiation trajectory in the pseudotime analysis using the Monocle 2 package (version 2.6.4; Monocle, USA).[21] We used the normalized expression cells × genes matrix to create a starting subject *CellDataSet class*.[22] We used the *differentialGeneTest* function to identify specific genes across multiple cell subtypes and applied the *orderCells* function for cell ordering in pseudotime. We implemented the DDRTree approach in the *reduceDimension* function for dimension reduction. We applied the *plot_cell_trajectory* function to map the trajectory in a two-dimensional space, with the two dimensions together presenting the cell differentiation state. The branches in the single-cell trajectories indicate different biologic functions depending on the gene expression during development. We identified key genes in different cell states using the cutoff value of false discovery rate less than 1e-5.[15]

Differentially Expressed Gene and Enrichment Analysis

We identified the differentially expressed genes within each cell type between the control and sevoflurane groups using the *FindMarkers* function in the Seurat. The differentially expressed genes were uncovered using the Model-based Analysis of Single-cell Transcriptomics,[23] based on the following criteria: |log$_2$(fold change)| 0.585 or greater, q value 0.05 or less, and the percentage of cells in the specific cluster greater than 25%.[24] We generated the heatmaps of differentially expressed genes using the z-score approach.

In addition, we performed the Gene Ontology enrichment analysis to provide all Gene Ontology terms (Cellular Component, Molecular Function, and Biologic Process) with significant enrichment of peak related differentially expressed genes in each cell type.[25] All peak related genes were mapped to Gene Ontology terms in the database (https://www.geneontology.org/). We also performed enrichment analysis of pathways based on the Kyoto Encyclopedia of Genes and Genomes database (https://www.genome.jp/kegg/) to identify significantly enriched metabolic pathways or signal transduction pathways with peak related differentially expressed genes in each cell type.[26] For the Gene Ontology and Kyoto Encyclopedia of Genes and Genomes enrichment analyses, the P value is calculated as follows: $p = 1 - \sum_{i=0}^{m-1} \frac{\binom{M}{i}\binom{N-M}{n-i}}{\binom{N}{n}}$,

in which N is the number of all genes with Gene Ontology/Kyoto Encyclopedia of Genes and Genomes annotation, *n* is the number of differentially expressed genes in N, M is the number of all genes annotated to the certain Gene Ontology terms or specific pathways, and *m* is the number of differentially expressed genes in M. The calculated P values were corrected using false discovery rate, with false discovery rate 0.05 or less as a threshold to determine a significantly enriched Gene Ontology terms or Kyoto Encyclopedia of Genes and Genomes pathways.

RNA *In Situ* Hybridization

The fresh hippocampal samples were fixed in 4% paraformaldehyde for 2h at 4°C. The samples were then embedded in paraffin and sectioned into 8-μm slices at room temperature. The sections were dehydrated with sequential washes with 50%, 75%, and 100% ethanol in phosphate buffered saline for 5min each. Rehydration was performed with sequential washes with 100%, 75%, and 50% ethanol. The sections were permeated for 2h in 1%Triton–X and washed three times with 0.1% Tween in phosphate buffered saline for 5min at room temperature. After prehybridization with probe hybridization buffer for 2h at 37°C, the sections were hybridized overnight at 37°C with the probes (RiboBio, China) that bound to the following target RNA: *Dcc* (lnc102941), *Grid1* (lnc102942), *Shank2* (lnc102939), *Ctnnd2* (lnc102943), *Pcdh7* (lnc102937),

and *Sobp* (lnc102938). Next, the sections were washed twice with 2 × standard saline citrate solution for 5min each, 0.5 × standard saline citrate solution for 15min, and 0.2 × standard saline citrate solution for 15min at 37°C. The cell nuclei were counterstained with 4',6-diamidino-2-phenylindole. The sections were treated with strept actividin-biotin complex –fluorescein isothiocyanate for 30min at 37°C. Fluorescent images were obtained at 400 × and 100 × magnification (Leica Aperio VERSA; Germany) using the Axiovision software (Carl Zeiss Vision, version 4.6). The results were analyzed with the fluorescence *in situ* hybridization quantification assay using the Image-Pro Plus software (version 6.0, Media Cybernetics, Inc., USA). The mean fluorescence intensity was calculated as integrated optical density/area (unit: pixel).

Real-time Quantitative Polymerase Chain Reaction

Total RNA was extracted from mice hippocampi using TRIZOL (ambion, USA). After RNA quantification and evaluation of RNA purity, cDNA was generated from RNA using a reverse transcription kit (TransGen Biotech, China). We performed the real-time quantitative polymerase chain reaction using the SYBR Green MasterMix (TransGen Biotech) in a reaction volume of 20 μl on the 7,500 Fast Real-Time Polymerase Chain Reaction System (Applied Biosystems, USA). The specific primers were designed and manufactured by Sangon Biotech (China) targeting *Dcc*, *Grid1*, *Shank2*, *Ctnnd2*, *Pcdh7*, and *Sobp*. The *GAPDH* was used as a reference gene. We recorded the cycle threshold value of each gene, and the gene abundance was calculated using the $2^{-\Delta\Delta \text{ (cycle threshold)}}$ method. The specific primers are as follows:

Mbp-forward, 5'-CCCACTTGATCCGCCTCTTT-3'
Mbp-reverse, 5'-CTCGGAGCTCACCTTGCC-3'
Mag-forward, 5'-GATGCCCTCGACCATCTCAG-3'
Mag-reverse, 5'-CGAACTGCAAGGTGGTGTTG-3'
Mog-forward,5'-GGTATCCCATCCGGGCTTTAG-3'
Mog-reverse, 5'-AGGTGCTTGCTCTGCATCTT-3'
Mal-forward, 5'-GTTTGTGAGTTTGATGCAGCCT-3'
Mal-reverse, 5'-GCTTCCAGAACTGAGGCACT-3'
GAPDH-forward,5'-GGTTGTCTCCTGCGACTTCA-3'
GAPDH-reverse,5'-TGGTCCAGGGTTTCTTACTCC-3'

Western Blot Analysis

Total protein of the hippocampus was extracted using the MT-cellytics and PIC 100X reagents (Biocolor BioScience, China). The proteins were separated using electrophoresis with 10% sodium dodecyl sulfate-polyacrylamide gel and transferred onto polyvinylidene fluoride membranes (Millipore Corp., USA). The membranes were blocked for 2h at room temperature. Next, the membranes were incubated with the primary antibodies at 4°C overnight: anti-glutamate ionotropic receptor delta type subunit 1 (1:50; 13040-1-AP; Proteintech) for glutamate ionotropic receptor delta type subunit 1 (100 to 112 kd), anti-delta-catenin (1:1,000; ab184917;

abcam) for delta-catenin (135 kd) encoded by *Ctnnd2*, anti–sine oculis binding protein homolog (1:1,000; OAAB00857; Aviva Systems Biology) for sine oculis binding protein homolog (92 kd), and anti–glyceraldehyde-3-phosphate dehydrogenase (1:2000; AF5009; Beyotime) for glyceraldehyde-3-phosphate dehydrogenase (37 kd). The membranes were incubated with horseradish peroxidase–conjugated secondary antibodies for 2h at room temperature. Glyceraldehyde-3-phosphate dehydrogenase was used as the loading control. The bands were visualized on the Tanon 5,200 system (Tanon, China).

Statistical Analysis

No statistical power calculation was conducted before the study. We determined the sample size based on a recent study (10 mice per group for behavioral tests, four to six mice per group for Western blot and real-time quantitative polymerase chain reaction, and three mice per group for immunostaining experiments).[5]

For the single-nucleus RNA sequencing data, we used R v3.5.3 (Foundation for Statistical Computing) for the statistical analyses and graphic generation. Bioinformatic tools were used to analyze cellular clustering, cross-talk, single-cell trajectory, differentially expressed genes, and enrichment. For the experimental data, we used GraphPad Prism software (version 9.0, USA) to perform statistical analyses and graphic plotting. We checked normal distribution of data using the Shapiro–Wilk test. The Morris water maze data are expressed as mean $\pm$ SD. We used Student's t test to analyze the between–group differences in platform–crossing times, time spent in the fourth quadrant, and mean distance from the platform. We used two–way repeated–measures ANOVA with Bonferroni correction to compare the two groups on escape latency, body weight, and body length. The expression of key genes in the trajectory analyses of dentate gyrus cell neurogenesis is expressed as mean $\pm$ SD (arbitrary units). We applied mixed-effect ANOVA (restricted maximum likelihood) with Geisser–Greenhouse correction to analyze the interaction between group and pseudotime, and multiple comparisons were corrected using the Bonferroni method. For the 24 common differentially expressed genes in male mice, we used Student's t test to analyze the between-group differences in their expression in specific hippocampal cell types. The data from fluorescence *in situ* hybridization quantification, real-time quantitative polymerase chain reaction, and Western blot are expressed as mean $\pm$ SD (arbitrary units), and we compared the two groups using Student's t test, mean difference, and 95% CI. There were no missing data for variables in this study. A P value <0.05 was considered statistically significant. All statistical tests were two-tailed.

Results

Identification of Hippocampal Cell Clusters with Novel Marker Genes of Both Sexes

Mice underwent control or sevoflurane treatment at postnatal days 6, 8, and 10, and the behavior tests showed that multiple neonatal exposures to sevoflurane resulted in significant learning and memory impairment in young mice of both sexes (Supplemental Digital Content, fig. 1, https://links.lww.com/ALN/D49). All mice survived until postnatal day 37, and then we performed data preprocessing and quality control (Supplemental Digital Content, fig. 2, https://links.lww.com/ALN/D49) and conducted single-nucleus RNA sequencing of the hippocampus.

For the identification of cell clusters, we compared our cluster-specific gene signatures of male mice (Supplemental Data 1, https://links.lww.com/ALN/D50) and female mice (Supplemental Data 2, https://links.lww.com/ALN/D51) to known markers of hippocampal cell types (Supplemental Digital Content, fig. 3, https://links.lww.com/ALN/D49).[16–19] The common markers for both sexes included *Slc1a3* (astrocytes), *Pex5l* (cornu ammonis 1 neurons), *Cpne4* (cornu ammonis 3 neurons), *Prox1* (dentate gyrus neurons), *Bsg* (endothelial cells), *Gad1* (γ-aminobutyric acid–mediated [GABAergic] neurons), *C1qa* (microglia), *MBP* (oligodendrocytes), and *Pdgfra* (oligodendrocyte precursor cells). Notably, our results revealed sex-specific cell type markers, including *Atp1a2* (astrocytes), *Tshz2* (cornu ammonis subtype neurons), *Reln* and *Nxph1* (cholinergic neurons), and *Acta2* (mural) for male mice, and *Rxfp1* (cornu ammonis subtype 1 neurons) and *Sulf1* (cornu ammonis subtype 2 neurons) for female mice.

For the male mice, we detected 15 hippocampal cell clusters including 23,806 hippocampal cell nuclei from the control male mice and 13,190 from the sevoflurane male mice (fig. 1A; Supplemental Data 1, https://links.lww.com/ALN/D50). For the female mice, we detected 12 hippocampal cell clusters including 25,402 hippocampal cell nuclei from the control female mice and 23,077 from the sevoflurane female mice (fig. 1B; Supplemental Data 2, https://links.lww.com/ALN/D51).

In male mice, the previously known cell markers exhibited cluster-specific expression, which validated our identification of specific hippocampal cell clusters (fig. 1C). After multiple sevoflurane exposures, the proportion of cornu ammonis 1 neurons was decreased from 79.9% to 32.3%, the proportion of dentate gyrus neurons was increased from 4.2% to 23.4%, and the proportion of oligodendrocytes was increased from 0.6% to 6.9% (fig. 1D). In contrast, no such changes in the proportion of cornu ammonis 1 neurons (from 27.3% to 24.3%), dentate gyrus neurons (from 36.2% to 35.8%), and oligodendrocytes (from 5.9% to 7.8%) were found in females (fig. 1E). For the female mice, the cell type–specific clusters were also validated by known cell markers (fig. 1F).

Our investigations also identified novel sex-specific marker genes for different hippocampal cell types. We showcased the top five highly expressed genes in male mice (Supplemental Digital Content, fig. 4A, https://links.lww.com/ALN/D49). For these genes, we examined cellular identity and visualized hippocampal localization by using the Allen Brain Atlas *in situ* hybridization images (https://mouse.brain-map.org)[18] (Supplemental Digital Content, figs. 5 to 9, https://links.lww.com/ALN/D49). Based on the expression of these top genes,
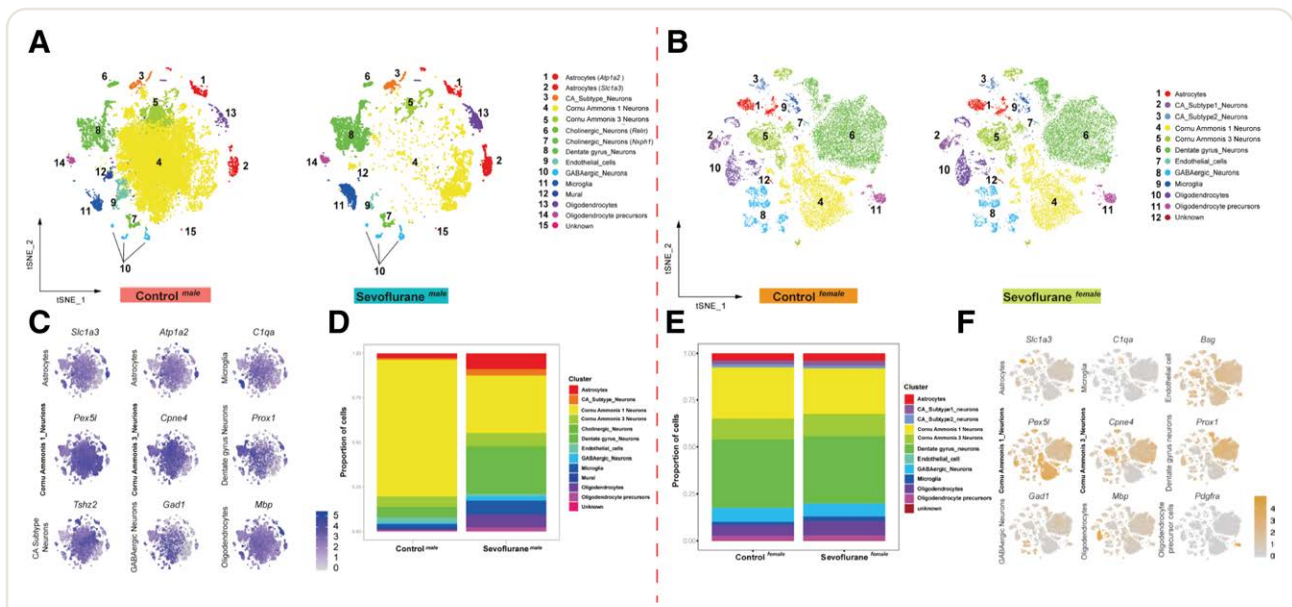
Fig. 1. Hippocampal cell clusters in male and female mice. (*A*) The t-distributed stochastic neighbor embedding plots showing 15 hippocampal cell clusters in the control male group (*left*) and sevoflurane male group (*right*). (*B*) The t-distributed stochastic neighbor embedding plots showing 12 hippocampal cell clusters in the control female group (*left*) and sevoflurane female group (*right*). (*C*) Expression of known cell markers in specific hippocampal clusters in males: astrocytes—*Slc1a3* and *Atp1a2*, microglia—*C1qa*, cornu ammonis 1 neurons—*Pex5l*, cornu ammonis 3 neurons—*Cpne4*, dentate gyrus neurons—*Prox1*, cornu ammonis subtype neurons—*Tshz2*, γ-aminobutyric acid–mediated (GABAergic) neurons—*Gad1*, and oligodendrocytes—*Mbp*. (*D*) The percentage of cells in specific hippocampal clusters in the control male and sevoflurane male groups. (*E*) The percentage of cells in specific hippocampal clusters in the control female and sevoflurane female groups. (*F*) Expression of known cell markers in specific hippocampal clusters in females: astrocytes—*Slc1a3*, microglia—*C1qa*, endothelial cells—*Bsg*, cornu ammonis 1 neurons—*Pex5l*, cornu ammonis 3 neurons—*Cpne4*, dentate gyrus neurons—*Prox1*, GABAergic neurons—*Gad1*, oligodendrocytes—*Mbp*, and oligodendrocyte precursor cells—*Pdgfra*.

we identified several novel marker genes in the male mice (*Gli2* for astrocytes, *Gm49906* for cornu ammonis subtype neurons, *Gm2629* for microglia, and *4930420G21Rik* for oligodendrocytes; Supplemental Digital Content, fig. 4B, https://links.lww.com/ALN/D49). For the female mice, we presented the top five highly expressed genes (Supplemental Digital Content, fig. 4C, https://links.lww.com/ALN/D49) and identified several novel marker genes (*Gm32647* for cornu ammonis 3 neurons, *Dlx6os1* for GABAergic neurons, and *Prr5l* for oligodendrocytes; Supplemental Digital Content, fig. 4D, https://links.lww.com/ALN/D49). These novel marker genes showed sex-specific differences and may help to uncover the characteristics and function of specific hippocampal cell types.

Sevoflurane Induced Sex-specific Alterations of Hippocampal Cellular Cross-talk

We investigated the hippocampal cellular cross-talk and focused on the trisynaptic circuit of the hippocampus (cornu ammonis 1, cornu ammonis 3, and dentate gyrus) during multiple sevoflurane exposures of both sexes. For the male mice, sevoflurane exposures enhanced the mutual interactions among cornu ammonis 1, cornu ammonis 3, and dentate gyrus, with increased numbers of significantly enriched

ligand–receptor pairs in all interactions (from 18 to 42 in cornu ammonis 1–cornu ammonis 3, from 21 to 35 in cornu ammonis 1–dentate gyrus, from 25 to 45 in cornu ammonis 3–dentate gyrus, from 8 to 32 in cornu ammonis 3–cornu ammonis 3, and from 14 to 16 in dentate gyrus–dentate gyrus; fig. 2A; Supplemental Data 3, https://links.lww.com/ALN/D52). Our results showed specific expression patterns of the top 25 ligand–receptor interactions (fig. 2B).

For the female mice, sevoflurane exposures increased the number of significantly enriched ligand–receptor pairs from 15 to 21 in cornu ammonis 1–cornu ammonis 3, from 12 to 20 in cornu ammonis 1–dentate gyrus, and from 17 to 20 in cornu ammonis 3–dentate gyrus, while the number of ligand–receptor pairs remained 20 in cornu ammonis 3–cornu ammonis 3 and 11 in dentate gyrus–dentate gyrus (fig. 2C; Supplemental Data 4, https://links.lww.com/ALN/D53). Sevoflurane exposures altered the expression profile of the top 25 ligand–receptor interactions (fig. 2D).

In addition, we showcased the significantly enriched ligand–receptor interactomes among different hippocampal cell types in male mice (Supplemental Digital Content, fig. 10A, https://links.lww.com/ALN/D49; Supplemental Data 5, https://links.lww.com/ALN/D54) and cell–cell communication network diagrams (Supplemental Digital
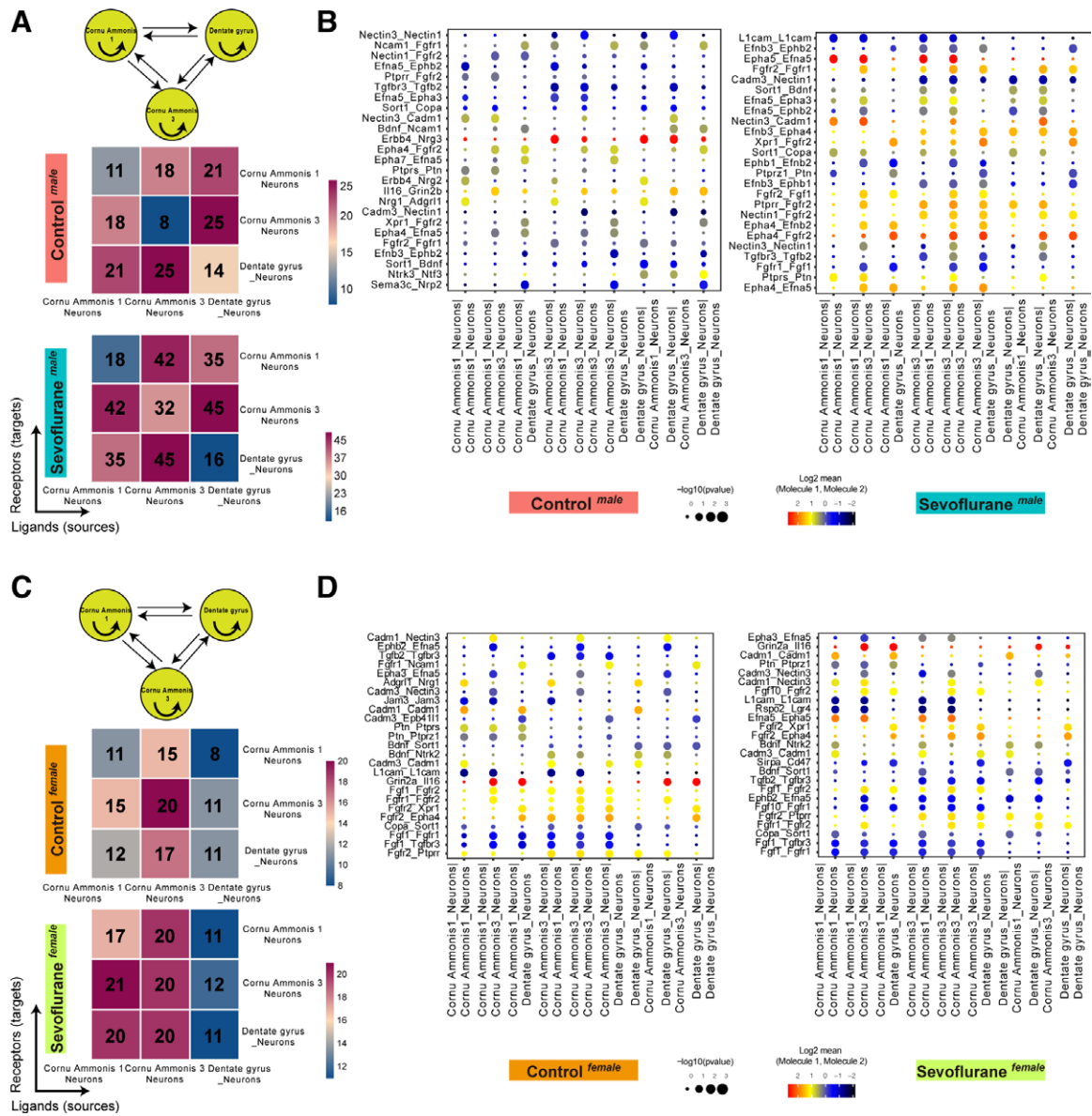
Fig. 2. Alterations in hippocampal trisynaptic circuit cellular cross-talk induced by sevoflurane exposures in male and female mice. (*A*) Heatmaps showing interactions among cornu ammonis 1, cornu ammonis 3, and dentate gyrus neurons in the control male group (*upper*) and sevoflurane male group (*lower*). The number of significant enriched ligand–receptor pairs is shown in each box. (*B*) Dot plots showing the top 25 enriched ligand–receptor interactions among cornu ammonis 1, cornu ammonis 3, and dentate gyrus neurons in the control male group (*left*) and sevoflurane male group (*right*). (*C*) Heatmaps showing interactions among cornu ammonis 1, cornu ammonis 3, and dentate gyrus neurons in the control female group (*upper*) and sevoflurane female group (*lower*). The number of significant enriched ligand–receptor pair is shown in each box. (*D*) Dot plots showing the top 25 enriched ligand–receptor interactions among cornu ammonis 1, cornu ammonis 3, and dentate gyrus neurons in the control female group (*left*) and sevoflurane female group (*right*). Dot size is proportional to the significance level of enriched ligand–receptors, and color intensity corresponds to the number of ligand–receptors. Criteria for significant enriched ligand–receptor pair: mincell_pct 30% or greater and *P* value <0.05 (CellPhoneDB software).

Content, fig. 10B, https://links.lww.com/ALN/D49). Sevoflurane also resulted in obvious changes in ligand–receptor gene regulatory interactions in female mice (Supplemental Digital Content, fig. 10, C and D, https://links.lww.com/ALN/D49; Supplemental Data 6, https://links.lww.com/ALN/D55).

Sevoflurane Led to Sex-specific Interruption of Dentate Gyrus Granule Cell Neurogenesis

Neurogenesis of dentate gyrus granule cells throughout postnatal life plays a critical role in various physiologic and pathophysiological conditions.[27] However, evidence is scant on the neurogenesis of dentate gyrus granule cells in developmental
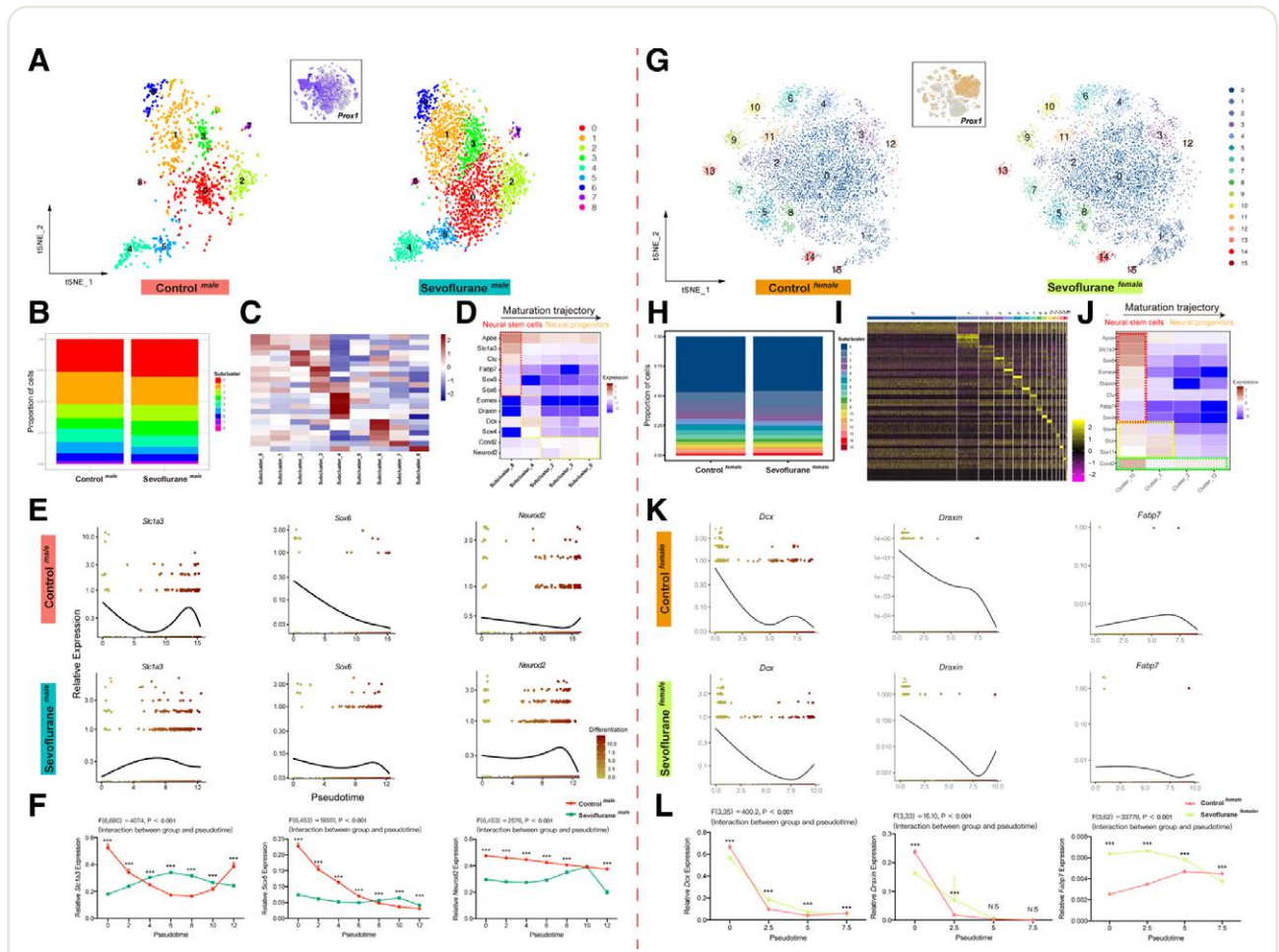
Fig. 3. Interruptions of dentate gyrus granule cell neurogenesis induced by sevoflurane exposures in male and female mice. (*A*) The t-distributed stochastic neighbor embedding plots showing nine dentate gyrus granule cell subclusters in the control male group (*left*) and sevoflurane male group (*right*). (*B*) The percentage of cells in specific dentate gyrus granule subclusters in the control male and sevoflurane male groups. (*C*) Heatmap showing the expression of specific marker genes for dentate gyrus granule subclusters. Criteria for specific marker genes: mincell_pct 0.25 or greater, *P* value ≤ 0.01, and log$_2$(fold change) 0.361 or greater (Seurat R package). (*D*) Heatmap showing the expression of specific marker genes (*rows*) in subclusters (*columns*) along the maturation trajectory from neural stem cells to neural progenitors. (*E*) Pseudotime expression graphs of representative specific marker genes (*Slc1a3*, *Sox6*, and *Neurod2*) showing the development profile of dentate gyrus granule cells in the control male group (*upper*) and sevoflurane male group (*lower*). Color intensity corresponds to the states of neurogenesis. (*F*) Interrupted expression of *Slc1a3* [$F_{(6,680)}$ = 4,074, $P < 0.001$], *Sox6* [$F_{(6,453)}$ = 18,551, $P < 0.001$], and *Neurod2* [$F_{(6,453)}$ = 2,576, $P < 0.001$] along the pseudotime course. Data are mean ± SD. n = 863 cells (control male) and n = 2,288 cells (sevoflurane male). Mixed-effect ANOVA with Bonferroni correction. ***$P < 0.001$. (*G*) The t-distributed stochastic neighbor embedding plots showing 16 dentate gyrus granule cell subclusters in the control female group (*left*) and sevoflurane female group (*right*). (*H*) The percentage of cells in specific dentate gyrus granule cell subclusters in the control female and sevoflurane female groups. (*I*) Heatmap showing the expression of specific marker genes for dentate gyrus granule cell subclusters. Criteria for specific marker genes: mincell_pct 0.25 or greater, *P* value ≤ 0.01, and log$_2$(fold change) 0.361 or greater (Seurat R package). (*J*) Heatmap showing the expression of specific marker genes (*rows*) in subclusters (*columns*) along the maturation trajectory from neural stem cells to neural progenitors. (*K*) Pseudotime expression graphs of specific marker genes showing the development profile of dentate gyrus granule cells in the control female group (*left*) and sevoflurane female group (*right*). Color intensity corresponds to the states of neurogenesis. (*L*) Interrupted expression of *Dcx* [$F_{(3,35)}$ = 400.2, $P < 0.001$], *Draxin* [$F_{(3,33)}$ = 15.1, $P < 0.001$], and *Fabp7* [$F_{(3,62)}$ = 33,779, $P < 0.001$] along the pseudotime course. Data are mean ± SD. n = 6,894 cells (control female) and n = 6,676 cells (sevoflurane female). Mixed-effect ANOVA with Bonferroni correction. ***$P < 0.001$.

sevoflurane neurotoxicity. Thus, we explored the effects of multiple sevoflurane exposures on the maturation trajectory of dentate gyrus granule cells. The t-distributed stochastic neighbor embedding plots detected nine subclusters of dentate gyrus granule cells in the male mice (fig. 3A). The sevoflurane exposures changed the proportions of subcluster 0 from 26.1% to 30.2% and subcluster 1 from 26.0% to 22.9% (fig. 3B). To

investigate the function of the subclusters, we analyzed their specific marker genes (fig. 3C; Supplemental Data 7, https://links.lww.com/ALN/D56). Based on the literature, dentate gyrus granule cell populations consist of neural stem cells (expressing *Apoe*, *Slc1a3*, *Clu*, *Fabp7*, *Sox9*, and *Sox6*), neural progenitors (expressing *Eomes*, *Draxin*, *Dcx*, *Sox4*, *Ccnd2*, and *Neurod2*), and mature granule cells (expressing *Gria1*), together

constituting the neurogenic lineage.[17] We then analyzed the maturation trajectory of dentate gyrus granule cells, showing the gene expression of subcluster 8 (neural stem cells) and subclusters 4, 2, 3, and 0 (neural progenitors) along with the temporal axis (fig. 3D). Based on subclusters 8, 4, 2, 3, and 0, the pseudotime analysis showed that sevoflurane exposures significantly interrupted the expression of $Slc1a3$ [$F(6,680) = 4,074$, $P < 0.001$], $Sox6$ [$F(6,453) = 18,551, P < 0.001$], and $Neurod2$ [$F(6,453) = 2,576, P < 0.001$] along the transition from neural stem cells to neural progenitors (fig. 3, E and F; Supplemental Data 8, https://links.lww.com/ALN/D57).

For the female mice, the t-distributed stochastic neighbor embedding plots illustrated 16 dentate gyrus granule cell subclusters (fig. 3G), without obvious changes in the proportions (fig. 3H). We also identified the specific marker genes (fig. 3I; Supplemental Data 9, https://links.lww.com/ALN/D63 and https://links.lww.com/ALN/D64) to analyze the maturation trajectory from subcluster 15 (neural stem cells) to 1, 2, and 12 (neural progenitors) (fig. 3J). Sevoflurane exposures significantly interrupted the expression of Dcx [$F(3,35) = 400.2$, $P < 0.001$], $Draxin$ [$F(3,33) = 15.1, P < 0.001$], and $Fabp7$ [$F(3,62) = 33,779, P < 0.001$] in the pseudotime analysis (fig. 3, K and L; Supplemental Data 8, https://links.lww.com/ALN/D57). Thus, sevoflurane exposures led to sex-specific interruption of dentate gyrus granule cell neurogenesis, with significant changes in males but small changes in females.

Sevoflurane Resulted in Sex-specific Inhibition of Microglia Differentiation

Microglia are the main neuroimmune cells. The differentiation of microglia determines several essential functions, including synaptic pruning and remodeling, nerve regeneration and repairment, and pro- and anti–inflammatory effects.[28] We explored the impact of multiple sevoflurane exposures on microglia differentiation. The t-distributed stochastic neighbor embedding plots showed three microglia subclusters in the male mice (fig. 4A). Sevoflurane exposures increased the proportion of subcluster 0 from 83.4% to 96.3% (fig. 4B). The functions of these subclusters were defined based on known marker genes.[28] The subcluster 0 (expressing $P2yr12$, $Cx3cr1$, and $Trem2$) was related to sensing cellular injury, synaptic pruning, and promotion of inflammation, while the subcluster 1 (expressing $Cd163$ and $Igf1$) and subcluster 2 (expressing $Mrc1$ and $Cd163$) functioned to enhance nerve regeneration and repair (fig. 4C; Supplemental Data 7, https://links.lww.com/ALN/D56).[28–32] In the differentiation trajectory of microglia, different branches correspond to different cell states and functions. Microglia differentiated from the subcluster 0 to 1 and 2 in normal conditions. However, microglia almost all stayed in the subcluster 0 in the sevoflurane group, suggesting that multiple sevoflurane exposures hampered microglia differentiation (fig. 4D). We also identified many key genes that determined the differentiation branches of microglia

(Supplemental Digital Content, fig. 11, https://links.lww.com/ALN/D49).

For the female mice, the t-distributed stochastic neighbor embedding plots showed two microglia subclusters (fig. 4E). The proportion of subcluster 0 was slightly changed from 92.4% to 89.4% (fig. 4F). Based on the marker genes (fig. 4G; Supplemental Data 9, https://links.lww.com/ALN/D63 and https://links.lww.com/ALN/D64), we defined the functions of the subclusters. The sevoflurane female group showed almost no changes in the microglia differentiation trajectory (fig. 4H). The Kyoto Encyclopedia of Genes and Genomes pathway enrichment analysis suggested that the subcluster 0 was related to the nervous system, and the subcluster 1 was related to the immune system (Supplemental Digital Content, fig. 12, https://links.lww.com/ALN/D49). Thus, sevoflurane exposures resulted in sex-specific inhibition of microglia differentiation, with remarkable changes in males but almost no changes in females.

Sevoflurane Caused Sex-specific Reduction in Cornu Ammonis 1 Pyramidal Cell Diversity

Cornu ammonis 1 pyramidal cells exhibit a high level of diversity, which plays key roles in spatial navigation and memory circuit.[33] Whether multiple neonatal sevoflurane exposures affect the diversity of cornu ammonis 1 neurons remains unknown. We discovered the patterns of cornu ammonis 1 cell diversity using the t-distributed stochastic neighbor embedding analysis to reveal 19 cornu ammonis 1 pyramidal cell subclusters in the male mice (fig. 5A). The proportion of the subcluster 0 was remarkably decreased from 41.8% to 5.8% (fig. 5B). We visualized the cornu ammonis 1 pyramidal cell states using the pseudotime approach. There were 11 states in the control mice, suggesting the cell diversity in the normal condition. However, multiple sevoflurane exposures eliminated this diversity, leaving three states only (fig. 5C). To further uncover the key genes underlying this phenomenon, we assessed the expression of the top genes ($Cacnb2$, $Cst3$, $Dpp10$, $Lingo2$, $Lrrc4c$, and $Tshz2$) in different states (fig. 5D; Supplemental Data 10, https://links.lww.com/ALN/D58). $Cacnb2$ was the top gene in state 1 of both groups. $Dpp10$, $Lingo2$, $Lrrc4c$, and $Tshz2$ were the top genes in state 2 of the sevoflurane male group and in state 8 of the control male group. $Cst3$ was the top gene in state 3 of the sevoflurane male group and in state 6 of the control male group. Thus, the three states (1, 2, and 3) in the sevoflurane male group appeared to be representative of the three states (1, 8, and 6) in the control male group.

For the female mice, the t-distributed stochastic neighbor embedding plots showed 14 cornu ammonis 1 pyramidal cell subclusters (fig. 5E), and the proportion of the subclusters remained unchanged after sevoflurane treatment (fig. 5F). By visualizing the cornu ammonis 1 pyramidal cell states, the two female groups had similar cell
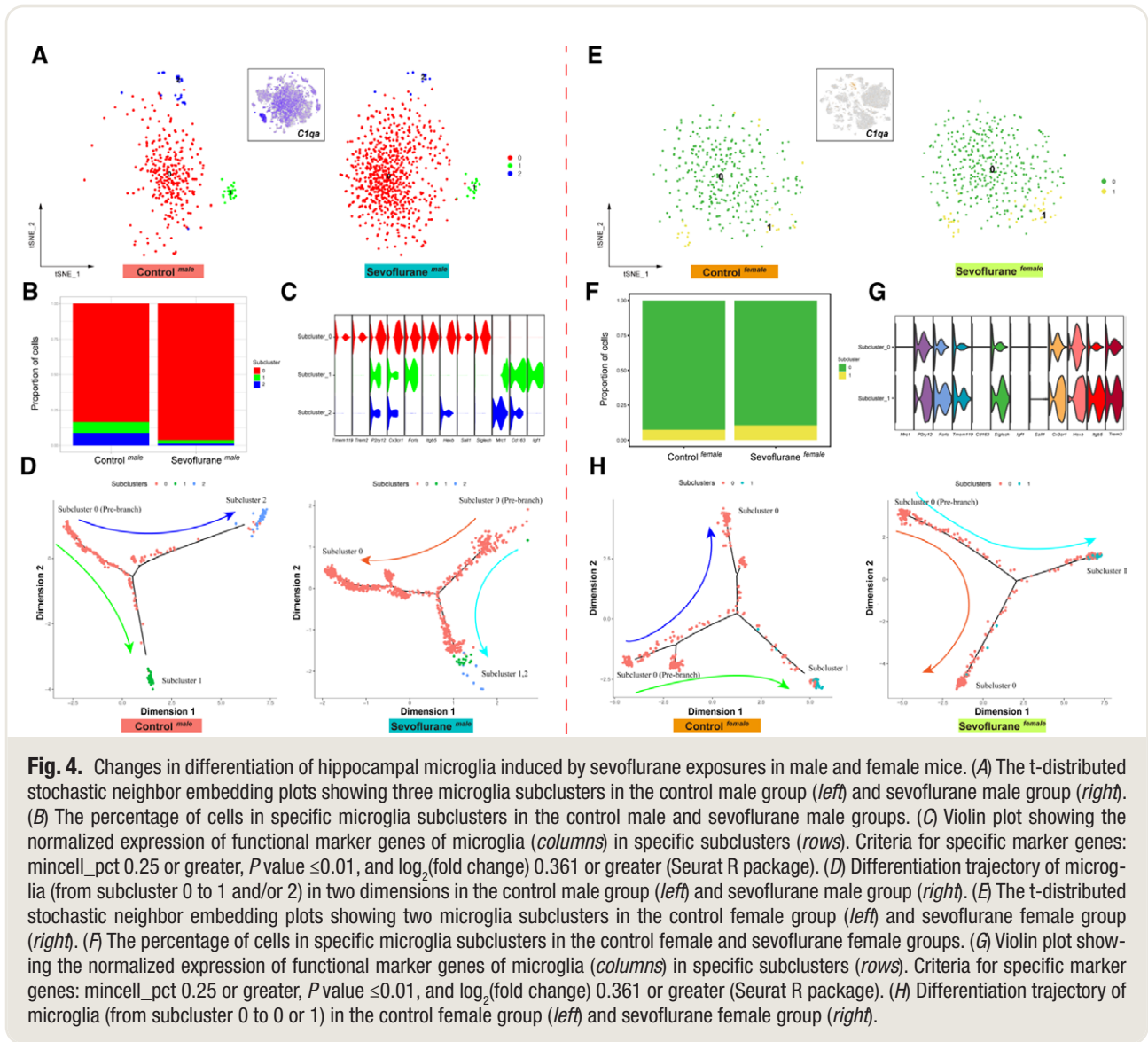
Fig. 4. Changes in differentiation of hippocampal microglia induced by sevoflurane exposures in male and female mice. (*A*) The t-distributed stochastic neighbor embedding plots showing three microglia subclusters in the control male group (*left*) and sevoflurane male group (*right*). (*B*) The percentage of cells in specific microglia subclusters in the control male and sevoflurane male groups. (*C*) Violin plot showing the normalized expression of functional marker genes of microglia (*columns*) in specific subclusters (*rows*). Criteria for specific marker genes: mincell_pct 0.25 or greater, *P* value ≤0.01, and log$_2$(fold change) 0.361 or greater (Seurat R package). (*D*) Differentiation trajectory of microglia (from subcluster 0 to 1 and/or 2) in two dimensions in the control male group (*left*) and sevoflurane male group (*right*). (*E*) The t-distributed stochastic neighbor embedding plots showing two microglia subclusters in the control female group (*left*) and sevoflurane female group (*right*). (*F*) The percentage of cells in specific microglia subclusters in the control female and sevoflurane female groups. (*G*) Violin plot showing the normalized expression of functional marker genes of microglia (*columns*) in specific subclusters (*rows*). Criteria for specific marker genes: mincell_pct 0.25 or greater, *P* value ≤0.01, and log$_2$(fold change) 0.361 or greater (Seurat R package). (*H*) Differentiation trajectory of microglia (from subcluster 0 to 0 or 1) in the control female group (*left*) and sevoflurane female group (*right*).
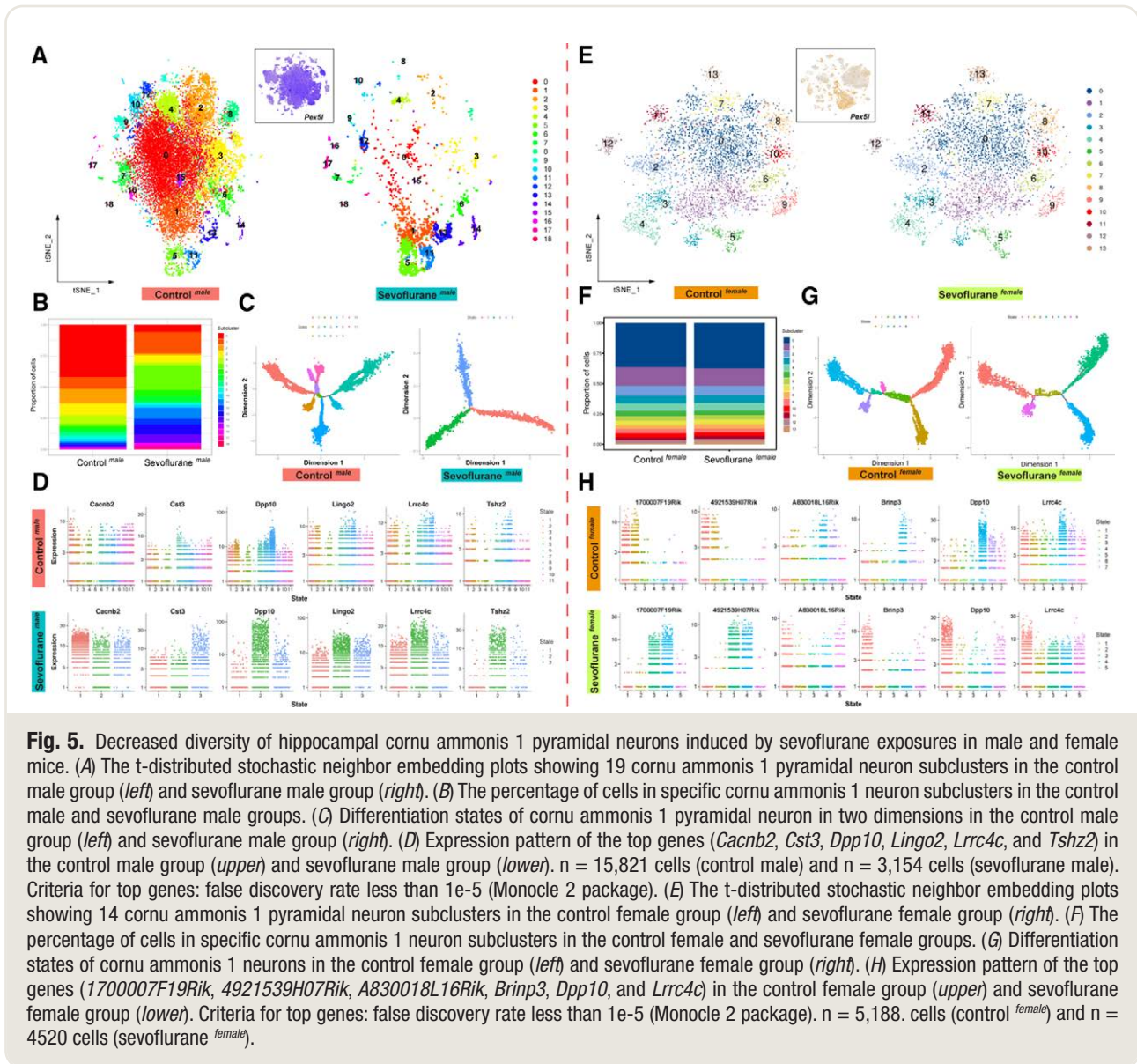
diversity profiles (fig. 5G). We also assessed the expression of the top genes in different cell states and found that the five states of the sevoflurane female group corresponded to the states of the control female group (fig. 5H; Supplemental Data 10, https://links.lww.com/ALN/D58). Therefore, sevoflurane exposures caused sex-specific reduction in cornu ammonis 1 pyramidal cell diversity, with dramatic changes in males but small changes in females.

Sevoflurane Induced Sex-specific Differentiation of Oligodendrocytes

Oligodendrocytes arise from oligodendrocyte precursor cells, which influence the generation and myelination of oligodendrocytes;[34] however, the sex-specific effects of

sevoflurane exposures on the differentiation of oligodendrocytes have not been reported. In the male mice, we analyzed the differentiation trajectory from oligodendrocyte precursor cells to oligodendrocytes (fig. 6A). The results showed that both the control male and sevoflurane male groups had three cell differentiation states (fig. 6B). In addition, we explored the mRNA expression of *Mbp*, *Mag*, *Mal*, and *Mog* (known cell markers of oligodendrocytes), showing that the expression of these four marker genes was comparable between the two groups (fig. 6C).

For the female mice, we visualized the differentiation trajectory (fig. 6D) to show that the number of oligodendrocyte states increased from three to five in the sevoflurane female group (fig. 6E). The Gene Set Enrichment Analysis enrichment plot suggested that most upregulated differentially expressed genes were enriched in

Fig. 5. Decreased diversity of hippocampal cornu ammonis 1 pyramidal neurons induced by sevoflurane exposures in male and female mice. (*A*) The t-distributed stochastic neighbor embedding plots showing 19 cornu ammonis 1 pyramidal neuron subclusters in the control male group (*left*) and sevoflurane male group (*right*). (*B*) The percentage of cells in specific cornu ammonis 1 neuron subclusters in the control male and sevoflurane male groups. (*C*) Differentiation states of cornu ammonis 1 pyramidal neuron in two dimensions in the control male group (*left*) and sevoflurane male group (*right*). (*D*) Expression pattern of the top genes (*Cacnb2, Cst3, Dpp10, Lingo2, Lrrc4c,* and *Tshz2*) in the control male group (*upper*) and sevoflurane male group (*lower*). n = 15,821 cells (control male) and n = 3,154 cells (sevoflurane male). Criteria for top genes: false discovery rate less than 1e-5 (Monocle 2 package). (*E*) The t-distributed stochastic neighbor embedding plots showing 14 cornu ammonis 1 pyramidal neuron subclusters in the control female group (*left*) and sevoflurane female group (*right*). (*F*) The percentage of cells in specific cornu ammonis 1 neuron subclusters in the control female and sevoflurane female groups. (*G*) Differentiation states of cornu ammonis 1 neurons in the control female group (*left*) and sevoflurane female group (*right*). (*H*) Expression pattern of the top genes (*1700007F19Rik, 4921539H07Rik, A830018L16Rik, Brinp3, Dpp10,* and *Lrrc4c*) in the control female group (*upper*) and sevoflurane female group (*lower*). Criteria for top genes: false discovery rate less than 1e-5 (Monocle 2 package). n = 5,188. cells (control *female*) and n = 4520 cells (sevoflurane *female*).

the process of positive regulation of myelination (Gene Ontology: 0031643) (fig. 6F). The sevoflurane female group had significantly increased mRNA expression of *Mbp* (0.19 ± 0.01 *vs.* 0.15 ± 0.01; mean difference = 0.04; 95% CI, 0.03 to 0.06; $P < 0.001$) and *Mag* (0.16 ± 0.01 *vs.* 0.12 ± 0.01; mean difference = 0.04; 95% CI, 0.03 to 0.05; $P < 0.001$) compared to the control female group (fig. 6G). Thus, sevoflurane exposures induced sex-specific effects on oligodendrocyte differentiation, with significant changes in females but very small changes in males.

Identification of Cell Type–specific Differentially Expressed Genes

To determine key genes and signaling pathways during sevoflurane exposures, we identified differentially

expressed genes within each cell cluster in the male mice (table 1; Supplemental Data 11, see the Supplemental Digital Content section at the end of the article for links to the data). Annotations of the differentially expressed genes with enriched Gene Ontology and Kyoto Encyclopedia of Genes and Genomes pathways in main cell types may help to explain the fundamental pathogenesis of developmental sevoflurane neurotoxicity (Supplemental Data 12, https://links.lww.com/ALN/D59 and Data 13, https://links.lww.com/ALN/D60). We found that the majority of the differentially expressed genes were unique to specific cell types, such as 402 differentially expressed genes in endothelial cells and 262 differentially expressed genes in neurons (fig. 7A). Most differentially expressed genes in neuron cell types were subtype-specific, such as 127 differentially expressed
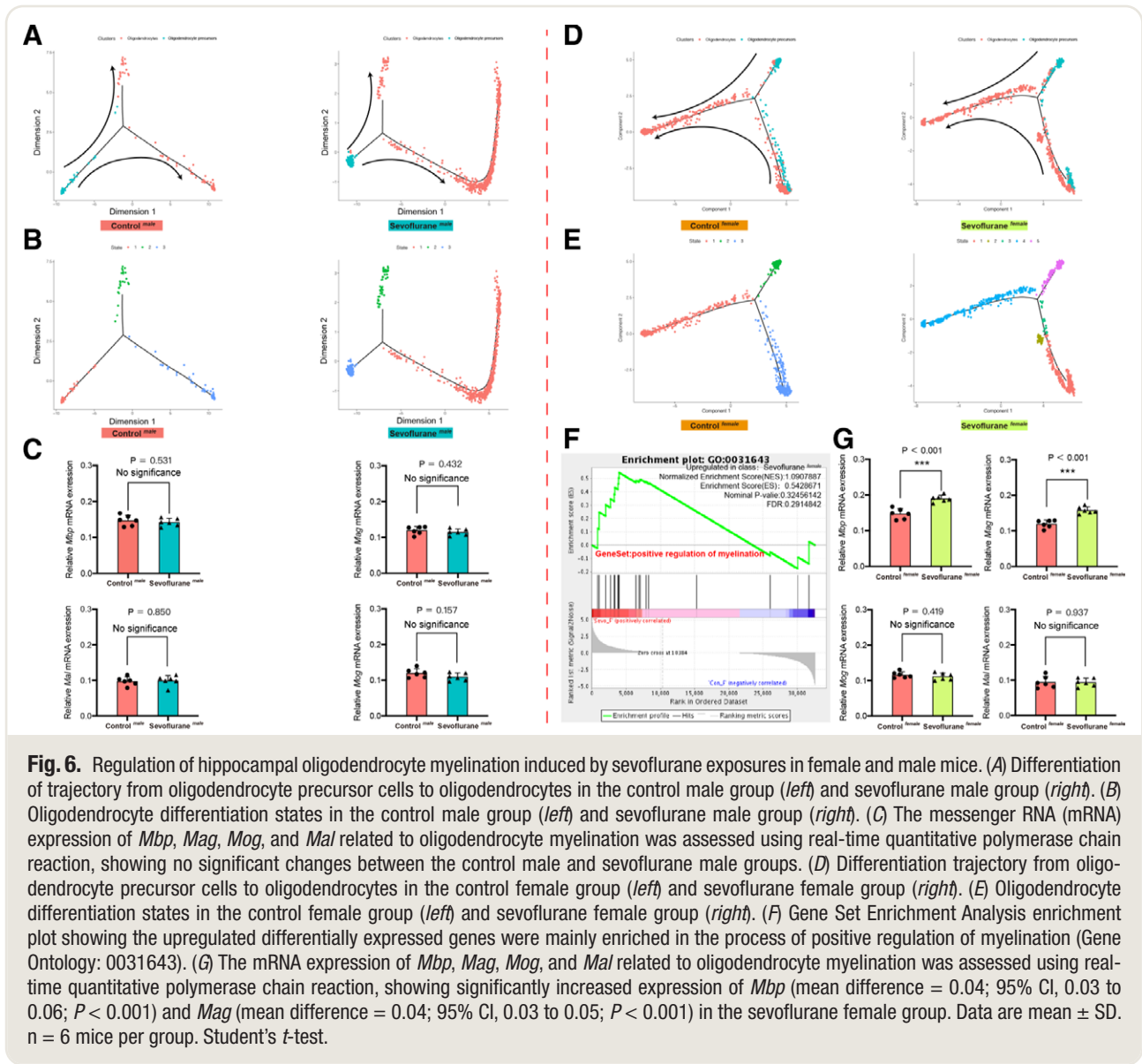
Fig. 6. Regulation of hippocampal oligodendrocyte myelination induced by sevoflurane exposures in female and male mice. (*A*) Differentiation of trajectory from oligodendrocyte precursor cells to oligodendrocytes in the control male group (*left*) and sevoflurane male group (*right*). (*B*) Oligodendrocyte differentiation states in the control male group (*left*) and sevoflurane male group (*right*). (*C*) The messenger RNA (mRNA) expression of *Mbp*, *Mag*, *Mog*, and *Mal* related to oligodendrocyte myelination was assessed using real-time quantitative polymerase chain reaction, showing no significant changes between the control male and sevoflurane male groups. (*D*) Differentiation trajectory from oligodendrocyte precursor cells to oligodendrocytes in the control female group (*left*) and sevoflurane female group (*right*). (*E*) Oligodendrocyte differentiation states in the control female group (*left*) and sevoflurane female group (*right*). (*F*) Gene Set Enrichment Analysis enrichment plot showing the upregulated differentially expressed genes were mainly enriched in the process of positive regulation of myelination (Gene Ontology: 0031643). (*G*) The mRNA expression of *Mbp*, *Mag*, *Mog*, and *Mal* related to oligodendrocyte myelination was assessed using real-time quantitative polymerase chain reaction, showing significantly increased expression of *Mbp* (mean difference = 0.04; 95% CI, 0.03 to 0.06; $P < 0.001$) and *Mag* (mean difference = 0.04; 95% CI, 0.03 to 0.05; $P < 0.001$) in the sevoflurane female group. Data are mean ± SD. n = 6 mice per group. Student's *t*-test.

genes in cornu ammonis 3 neurons and 96 differentially expressed genes in cornu ammonis 1 neurons (fig. 7B). By visualizing the expression patterns of these unique differentially expressed genes, we revealed clear differential expression profiles in the endothelial cells, neurons, astrocytes, cornu ammonis 3 neurons, and cornu ammonis 1 neurons (fig. 7C).

For the female mice, we identified differentially expressed genes within each hippocampal cell cluster (Supplemental Digital Content, fig. 13A, https://links.lww.com/ALN/D49; Supplemental Data 14, see the Supplemental Digital Content section at the end of the article for links to the data) and analyzed the enriched Gene Ontology and Kyoto Encyclopedia of Genes and Genomes pathways (Supplemental Data 15, https://links.lww.com/ALN/D61 and Data 16, see the Supplemental Digital Content section

at the end of the article for links to the data). The majority of the differentially expressed genes were also unique to specific cell types, such as 126 differentially expressed genes in oligodendrocytes and 379 differentially expressed genes in neurons (Supplemental Digital Content, fig. 13B, https://links.lww.com/ALN/D49). Most differentially expressed genes in neuron cell types were subtype-specific, such as 178 differentially expressed genes in cornu ammonis 3 neurons and 86 differentially expressed genes in cornu ammonis 1 neurons (Supplemental Digital Content, fig. 13C, https://links.lww.com/ALN/D49).

Validation of Common Differentially Expressed Genes

In our previous study, we utilized RNA sequencing to identify 314 hippocampal differentially expressed genes

Table 1. Number of Differentially Expressed Genes in Major Cell Types and Top Enriched Pathways

Cell Type	No. of Differentially Expressed Genes	Top Enriched Pathway	Representative Differentially Expressed Genes
Astrocytes	77 (up) 221 (down)	Endocytosis	Up: *Grk3, Arap2* Down: *Pld1, Pard3, Smad3, Tgfbr1, Smurf2, Igf1r, Grk5, Dnajc6, Dab2, Wipf1*
Microglia	11 (up) 12 (down)	Apelin signaling pathway	Down: *Gng2, Prkce*
Cornu ammonis 1 pyramidal neurons	78 (up) 97 (down)	Parkinson disease	Down: *mt-Cytb, mt-Atp6, mt-Co1, mt-Co2, mt-Co3, Cox8a, mt-Nd1, mt-Nd2, mt-Nd4, Ubb*
Cornu ammonis 3 pyramidal neurons	111 (up) 98 (down)	Alzheimer disease	Down: *mt-Cytb, mt-Atp6, Calm2, Calm1, mt-Co1, mt-Co2, mt-Co3, Cox8a, Apoe, Itpr1, Adam10*
Dentate gyrus granule neurons	17 (up) 5 (down)	Neuroactive ligand–receptor interaction	Up: *Htr1f, Glp2r*
Cornu ammonis subtype neurons	2 (up) 5 (down)	Synaptic vesicle cycle	Down: *Dnm3*
Cholinergic neurons	4 (up) 7 (down)	Alpha-linolenic acid metabolism	Up: *Pla2g3*
Endothelial cells	248 (up) 271 (down)	Glutamatergic synapse	Up: *Itpr², Plcb1, Plcb4,* Down: *Gria2, Grin2a, Adcy2, Shank2, Cacna1c*
Mural	9 (up) 4 (down)	Vascular smooth muscle contraction	Up: *Prkg1, Cald1*

Criteria for differentially expressed genes: mincell_pct 0.25 or greater, q value ≤ 0.05, and |log2(fold change)| 0.585 or greater (Model-based Analysis of Single-cell Transcriptomics test).

from the male mice subjected to multiple neonatal sevoflurane exposures.[11] Our current single-nucleus RNA sequencing in the male mice revealed a total of 1,035 differentially expressed genes, many of which were cell type–specific and cannot be retrieved from the whole-tissue analysis. There are 24 common differentially expressed genes between our previous whole-tissue results and the current single-cell genomic analysis (fig. 7D), which may be mechanistic driving forces for the sevoflurane-induced hippocampal cell type–specific effects during development in mice. We evaluated the expression of 24 common differentially expressed genes across main cell types (Supplemental Digital Content, fig. 14, https://links.lww.com/ALN/D49; Supplemental Data 11, see the Supplemental Digital Content section at the end of the article for links to the data).

The fluorescence *in situ* hybridization quantification assay was used to assess the mRNA expression and localization of six common differentially expressed genes related to neural function and memory. Our results showed increased expression of three common genes, as measured with mean fluorescence intensity: *Grid1* (0.12 ± 0.02 *vs.* 0.07 ± 0.01; mean difference = 0.05; 95% CI, 0.01 to 0.08; $P = 0.019$), *Ctnnd2* (0.13 ± 0.03 *vs.* 0.06 ± 0.01; mean difference = 0.07; 95% CI, 0.02 to 0.12; $P = 0.014$), and *Sobp* (0.13 ± 0.02 *vs.* 0.09 ± 0.02; mean difference = 0.04; 95% CI, 0.001 to 0.08; $P = 0.045$) (fig. 8). The Western blot showed that the protein expression of delta-catenin encoded by *Ctnnd2* was increased after sevoflurane treatment (1.94 ± 0.30 *vs.* 0.74 ± 0.23; mean difference = 1.20; 95% CI, 0.74 to 1.67;

$P < 0.001$; Supplemental Digital Content, fig. 15, https://links.lww.com/ALN/D49).

Discussion

In this single-cell nucleus RNA sequencing study, we identified novel sex-specific cell type marker genes in the hippocampus and demonstrated sex- and cell type–specific effects of sevoflurane on distinct hippocampal cell populations. In male but not in female mice, multiple neonatal sevoflurane exposure altered ligand–receptor interactomes in the trisynaptic hippocampal circuit of cornu ammonis 1, cornu ammonis 3, and dente gyrus, interfered with dentate gyrus granule cell neurogenesis, hampered microglia differentiation, and decreased cornu ammonis 1 pyramidal cell diversity. In contrast, oligodendrocyte differentiation was mainly altered in female but not in male mice.

To identify the cell clusters in our study, we compared our cluster-specific gene signatures to the known and published patterns of hippocampal cell types.[16–19] For the accuracy of the clusters in our study, we showed significant overlap between our defined cluster-specific genes and previously known markers. Next, we validated that our identified cell types fit into the Allen Brain Atlas data set by visualization of their hippocampal location. We also found an unknown cell cluster in either sex of mice, and the cell signatures have not been reported in the literature. Due to the small number of cells (66 cells in male mice and 135 cells in female mice) in these unknown clusters,
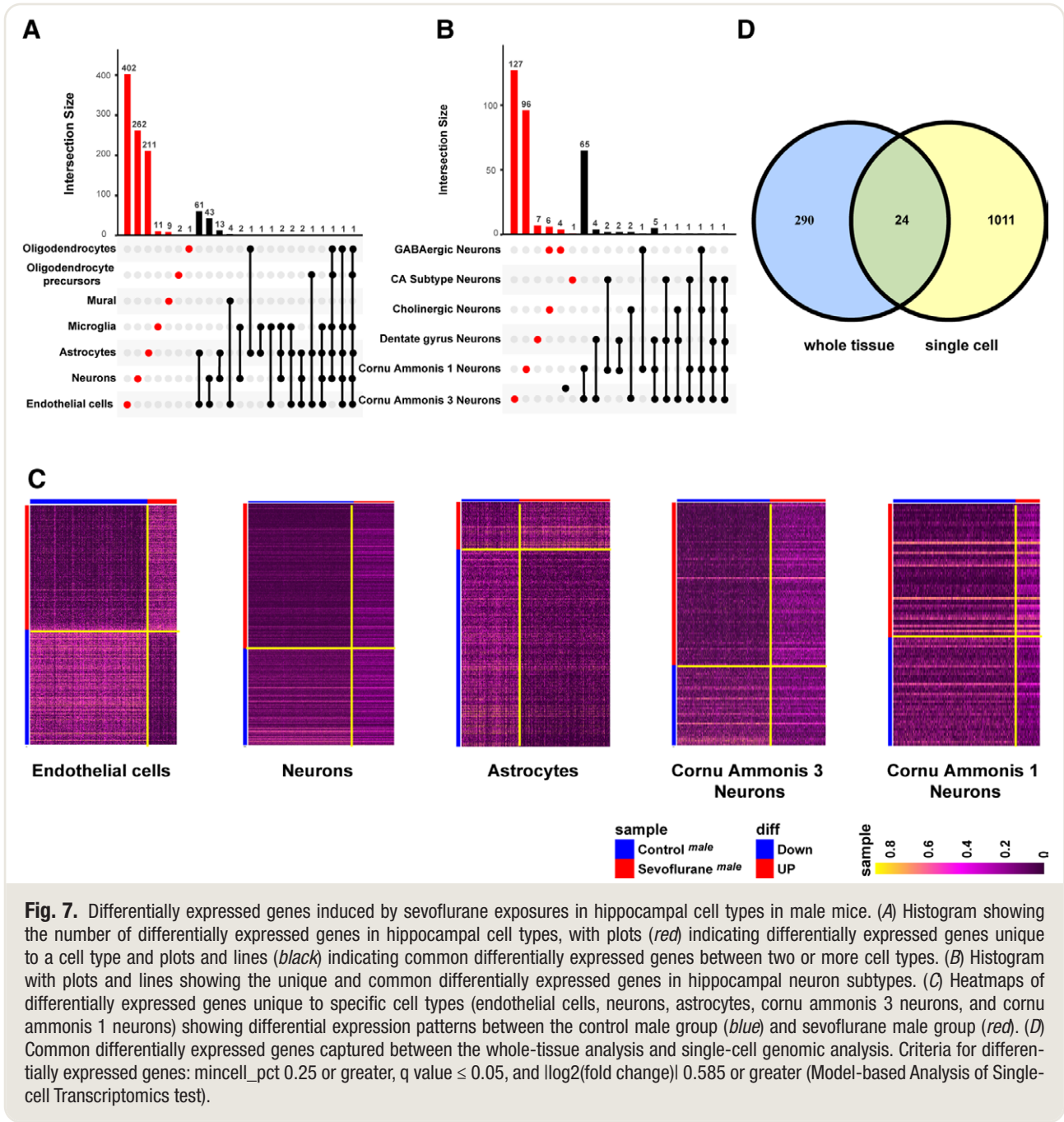
Fig. 7. Differentially expressed genes induced by sevoflurane exposures in hippocampal cell types in male mice. (*A*) Histogram showing the number of differentially expressed genes in hippocampal cell types, with plots (*red*) indicating differentially expressed genes unique to a cell type and plots and lines (*black*) indicating common differentially expressed genes between two or more cell types. (*B*) Histogram with plots and lines showing the unique and common differentially expressed genes in hippocampal neuron subtypes. (*C*) Heatmaps of differentially expressed genes unique to specific cell types (endothelial cells, neurons, astrocytes, cornu ammonis 3 neurons, and cornu ammonis 1 neurons) showing differential expression patterns between the control male group (*blue*) and sevoflurane male group (*red*). (*D*) Common differentially expressed genes captured between the whole-tissue analysis and single-cell genomic analysis. Criteria for differentially expressed genes: mincell_pct 0.25 or greater, q value ≤ 0.05, and |log2(fold change)| 0.585 or greater (Model-based Analysis of Single-cell Transcriptomics test).

we assume that they exert limited biologic function only. Nevertheless, further studies are required to assess their identity and function.

Emerging evidence suggests that the pathophysiological bases of many brain disorders can be accounted for by disturbances in the neurologic network, other than a small number of gene mutations or risk factors.[35] The perturbations in the interaction patterns among hippocampal neural circuits contributed to cognitive impairment in neurologic injury.[18] Currently, there is no evidence to show the changes in the interactions among different hippocampal neuronal and nonneuronal cell types after multiple neonatal

exposures to sevoflurane. We assessed the abundance of ligand–receptor interactions and uncovered the cell–cell communication relationship. We found significant shifts in the expression patterns of the hippocampal neural circuit, implicating a reorganization of the hippocampal network in response to sevoflurane. Based on these findings, our results point toward hippocampal circuit perturbations underlying sevoflurane exposures during development.

Neurogenesis in the hippocampus is restricted to the dentate gyrus subgranular zone and occurs constitutively throughout postnatal life.[27] Neural stem cells generate differentiated neural progenitor cells and ultimately produce
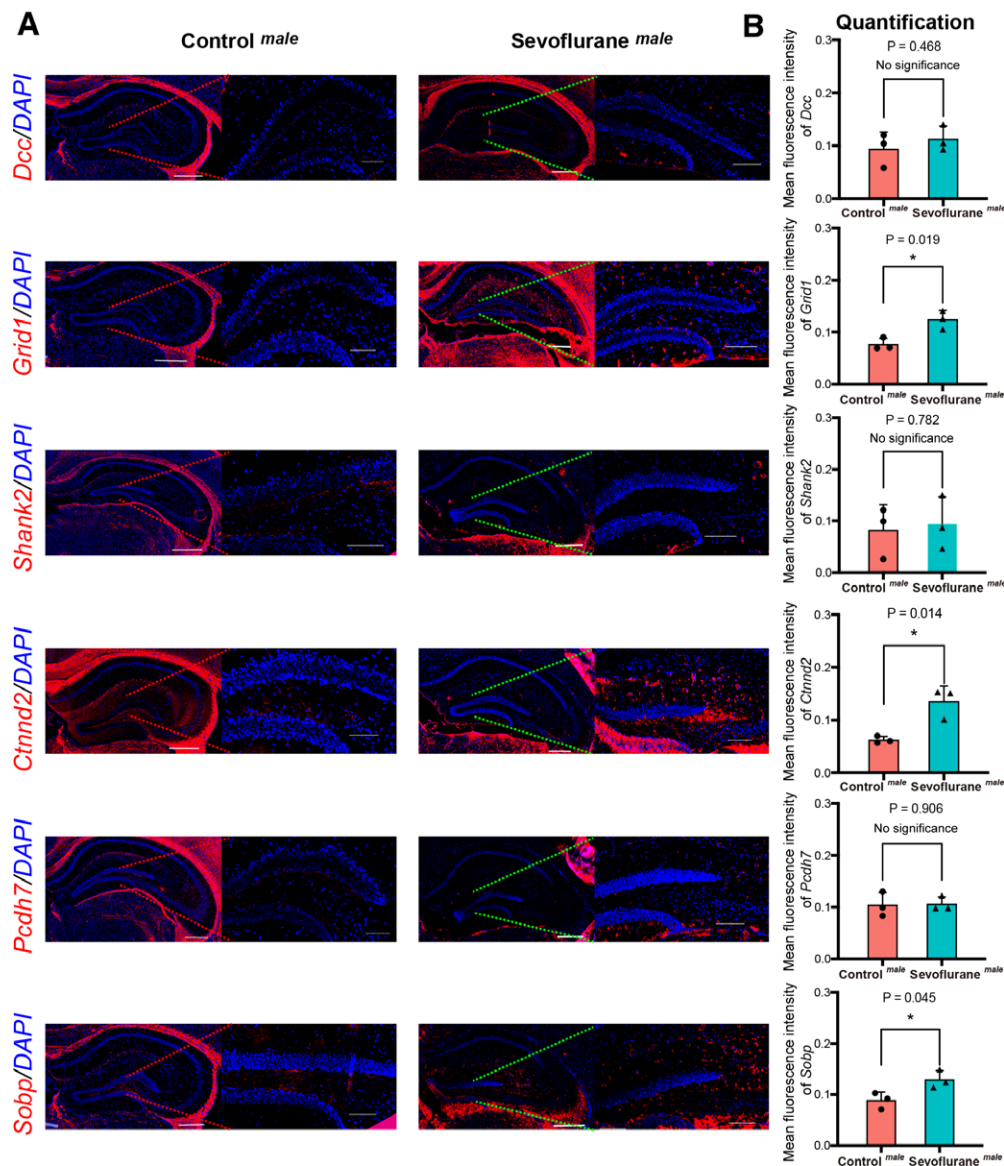
Fig. 8. Validation of select common differentially expressed genes in male mice using fluorescence *in situ* hybridization. (*A*) Fluorescence *in situ* hybridization images showing the expression of the hippocampus differentially expressed genes (*Dcc, Grid1, Shank2, Ctnnd2, Pcdh7,* and *Sobp*) in the control male group (*left*) and sevoflurane male group (*right*). Scale bars = 400 μm in low-magnification images and 100 μm in high-magnification images. (*B*) Fluorescence *in situ* hybridization quantification showing that the sevoflurane male group had upregulated expression of *Grid1* (mean difference = 0.05; 95% CI, 0.01 to 0.08; *P* = 0.019), *Ctnnd2* (mean difference = 0.07; 95% CI, 0.02 to 0.12; *P* = 0.014), and *Sobp* (mean difference = 0.04; 95% CI, 0.001 to 0.08; *P* = 0.045). Data are mean ± SD. n = 3 mice/group. Student's *t*-test.

mature granule neurons, which plays an essential role in cognitive function.[36] A recent study suggested that the ongoing hippocampal neurogenesis contributed to sustaining cognitive function throughout life, and the decreased neurogenesis with aging was associated with cognitive impairment or neuropsychiatric diseases.[37] In a rat model of anesthesia exposure, repeated neonatal sevoflurane treatments resulted in neurocognitive abnormalities, impaired proliferation of dentate gyrus neural progenitors, and decreased survival

of new granule cells.[7] In our study, different dentate gyrus granule cells (neural stem cells, neural progenitors, and mature granule cells) at different developmental stages were identified according to known hallmark genes. Sevoflurane exposures led to sex-specific interruption of dentate gyrus granule cell neurogenesis, with changes of different key genes related to dentate gyrus cell neurogenesis along the maturation trajectory, such as *Slc1a3, Sox6,* and *Neurod2* in male mice and *Dcx, Draxin,* and *Fabp7* in female mice.

As principal brain immune cells, microglia are related to homeostasis and host defense responses against pathogens in the central nervous system.[38] Previous RNA sequencing studies identified the microglia–specific markers in the brain related to essential functions: (1) sensing environment, (2) housekeeping, and (3) protection against infectious pathogens, injurious self-proteins, and tumor cells.[28,29] Microglia sense and scan the surrounding area constantly and polarize toward the injury area rapidly, and they are regulated by genes such as *P2yr12* and *Itgb5* in the subcluster 0 of the male mice in our results.[39] The housekeeping functions consist of synaptic remodeling, migration, and maintaining myelin homeostasis (involving *Cx3cr1* and *TREM2* in the subcluster 0).[30,31] Moreover, microglia exert protective functions to reduce inflammation and repair cell damage (involving *Mrc1*, *cd163*, and *Igf1* in the subclusters 1 and 2 of the male mice).[32] Thus, sevoflurane exposures blocked the process of microglia differentiation from the subcluster 0 to subclusters 1 and/or 2 in the male mice, which may lead to persistent neuroinflammation, neurotoxicity, and finally neurodegeneration. For the female mice, we identified two subclusters, with subcluster 0 related to the nervous system and 1 related to the immune system. Sevoflurane exposures led to only mild changes in the differentiation trajectory of microglia in female mice.

Cornu ammonis 1 pyramidal neurons with diverse differentiation states and the cornu ammonis 3–cornu ammonis 1 circuit are essential for memory processing and storage.[40] The existing clinical evidence showed that cognitive and memory declines were the most characteristic pathologic hallmarks in anesthetic–induced developmental neurotoxicity.[41] We found that multiple neonatal sevoflurane exposures considerably affected the pyramidal cells, particularly the cornu ammonis 1 neurons, with only minor effects on the GABAergic or cholinergic neurons. In the male mice, the differentiation states of cornu ammonis 1 cells were remarkably reduced to only three states after sevoflurane treatment compared with 11 states in the normal conditions. As the three states in the sevoflurane group were probably to be included in the control group, we assumed that sevoflurane exposures resulted in a narrowing of cornu ammonis 1 diversity outcome in male mice. In contrast, the female control and sevoflurane groups exhibited similar profiles of cornu ammonis 1 pyramidal cell diversity. Notably, while there was a dramatic loss of cornu ammonis 1 cell diversity in males, there was almost no change in females.

Oligodendrocytes derive from oligodendrocyte precursor cells, maintaining myelin integrity to retain fast electrical conduction and axonal support.[42] Recent studies have reported the effects of sevoflurane on myelinization. Zhang *et al.* reported that multiple sevoflurane exposures resulted in folate metabolism disruption and subsequently myelination defects in the developmental brain.[43] Fan *et al.* reported that maternal sevoflurane exposure blocked the development and maturation of oligodendrocytes in the hippocampus of offspring mice.[44] Our results suggested that sevoflurane exposures may affect hippocampal oligodendrocyte myelination in the female mice, but not in the male mice. This is evidenced by increased expression of *Mbp* and *Mag* in relation to positive regulation of myelination.

By analyzing the common differentially expressed genes between our previous whole-tissue study and the current single-cell genomic results, we found several multiple cell type differentially expressed genes in relation to neural function and memory. *Dcc* (the receptor deleted in colorectal cancer) and its ligand netrin-1 are essential for hippocampal synaptic plasticity and spatial memory.[45] *Grid1*, a member of the ionotropic glutamate receptor family, is crucial for normal synapse function, learning, and memory.[46] *Shank2*, coding a scaffolding protein expressed on the postsynaptic membrane of glutamatergic neurons, regulates the number of synapses, dendrite length and complexity, synaptic plasticity, and neuronal morphogenesis.[47] *Ctnnd2*, coding delta-catenin (a brain-specific protein), regulates dendritic complexity and dendritic spine density in the mature brain.[48] *Pcdh7* is highly expressed in the brain, which is related to the regulation of N–methyl-D-aspartate receptor currents and central nervous system disorders.[49] *Sobp*, encoding a nuclear zinc finger protein in the limbic system, is involved in intellectual disability.[50]

This study has several limitations. First, the Morris water maze test confirmed the successful establishment of cognitive impairment model in mice of both sexes. We showed similar cognitive behavioral disorders between the male and female mice; however, it is plausible that the underlying mechanisms are different at the cellular level. Thus, our results provide novel mechanistical insights for further investigations. Second, we assessed the sevoflurane-induced hippocampal cell type–specific effects at postnatal day 37 only. Including more timepoints for observation would have provided more information in the acute phase after multiple sevoflurane exposures. Third, the relatively low number of animals used in these experiments does not allow statistical comparison between males and females, but our data are suggestive of sex-specific effects. Next, because of the low number of animals per analysis, future experiments are still needed for the replication of our results and cluster solution. Last, the role of the key risk genes in specific hippocampal cell types identified in our study needs further investigation in functional studies, preferably using transgenic mice.

In conclusion, this single-nucleus RNA sequencing study offers a comprehensive hippocampal cell type atlas and transcriptional profiles in mice of both sexes after multiple neonatal exposures to sevoflurane. We discovered sex-specific perturbations in cellular cross-talk, dentate gyrus granule cell neurogenesis, microglia differentiation, cornu ammonis 1 neuron diversity, and oligodendrocyte myelination with novel risk genes that may serve as underlying mechanisms. The results of our study provide a valuable resource for sevoflurane-induced hippocampal neuronal and nonneuronal cell type–specific and sex-specific effects during development.

Correspondence

Address correspondence to Dr. Ji: Department of Anesthesiology, First Affiliated Hospital of Soochow University, 188 Shizi Street, Suzhou, Jiangsu 215006, China. jifuhaisuda@163.com. This article may be accessed for personal use at no charge through the Journal Web site, www.anesthesiology.org.

Supplemental Digital Content

Supplemental Figures: https://links.lww.com/ALN/D49
Supplemental Data 1. Details of cell clusters in male mice, https://links.lww.com/ALN/D50
Supplemental Data 2. Details of cell clusters in female mice, https://links.lww.com/ALN/D51
Supplemental Data 3. Interactions of cornu ammonis 1, cornu ammonis 3, and dentate gyrus in male mice, https://links.lww.com/ALN/D52
Supplemental Data 4. Interactions of cornu ammonis 1, cornu ammonis 3, and dentate gyrus in female mice, https://links.lww.com/ALN/D53
Supplemental Data 5. Ligand–receptor interactomes in male mice, https://links.lww.com/ALN/D54
Supplemental Data 6. Ligand–receptor interactomes in female mice, https://links.lww.com/ALN/D55
Supplemental Data 7. Marker genes of dentate gyrus subclusters in male mice, https://links.lww.com/ALN/D56
Supplemental Data 8. Pseudotime analysis of dentate gyrus neurogenesis, https://links.lww.com/ALN/D57
Supplemental Data 9. Marker genes of dentate gyrus subclusters in female mice, https://links.lww.com/ALN/D63, https://links.lww.com/ALN/D64
Supplemental Data 10. Key genes of cornu ammonis 1 cell diversity in male mice, https://links.lww.com/ALN/D58
Supplemental Data 11. Differentially expressed genes within each cell cluster in male mice, https://links.lww.com/ALN/D65, https://links.lww.com/ALN/D66, https://links.lww.com/ALN/D67, https://links.lww.com/ALN/D68, https://links.lww.com/ALN/D69, https://links.lww.com/ALN/D70, https://links.lww.com/ALN/D71, https://links.lww.com/ALN/D72
Supplemental Data 12. Gene Ontology terms of differentially expressed genes in male mice, https://links.lww.com/ALN/D59
Supplemental Data 13. Kyoto Encyclopedia of Genes and Genomes of differentially expressed genes in male mice, https://links.lww.com/ALN/D60
Supplemental Data 14. Differentially expressed genes within each cell cluster in female mice, https://links.lww.com/ALN/D73, https://links.lww.com/ALN/D74, https://links.lww.com/ALN/D75, https://links.lww.com/ALN/D76, https://links.lww.com/ALN/D77, https://links.lww.com/ALN/D78, https://links.lww.com/ALN/D79, https://links.lww.com/ALN/D80, https://links.lww.com/ALN/D81
Supplemental Data 15. Gene Ontology terms of differentially expressed genes in female mice, https://links.lww.com/ALN/D61
Supplemental Data 16. Kyoto Encyclopedia of Genes and Genomes of differentially expressed genes in female mice, https://links.lww.com/ALN/D82, https://links.lww.com/ALN/D83, https://links.lww.com/ALN/D84, https://links.lww.com/ALN/D85, https://links.lww.com/ALN/D86, https://links.lww.com/ALN/D87, https://links.lww.com/ALN/D88, https://links.lww.com/ALN/D89, https://links.lww.com/ALN/D90, https://links.lww.com/ALN/D91, https://links.lww.com/ALN/D92, https://links.lww.com/ALN/D93

References

1. Rice D, Barone S Jr.: Critical periods of vulnerability for the developing nervous system: Evidence from humans and animal models. Environ Health Perspect 2000; 108;(suppl 3):511–33
2. Liu X, Ji J, Zhao GQ: General anesthesia affecting on developing brain: Evidence from animal to clinical research. J Anesth 2020; 34:765–72
3. Cabrera OH, Gulvezan T, Symmes B, Quillinan N, Jevtovic-Todorovic V: Sex differences in neurodevelopmental abnormalities caused by early-life anaesthesia exposure: A narrative review. Br J Anaesth 2020; 124:e81–91
4. Lee BH, Chan JT, Kraeva E, Peterson K, Sall JW: Isoflurane exposure in newborn rats induces long-term cognitive dysfunction in males but not females. Neuropharmacology 2014; 83:9–17
5. Yu Y, Yang Y, Tan H, Boukhali M, Khatri A, Yu Y, Hua F, Liu L, Li M, Yang G, Dong Y, Zhang Y, Haas W, Xie Z: Tau contributes to sevoflurane-induced neurocognitive impairment in neonatal mice. Anesthesiology 2020; 133:595–610

6. Lu H, Liufu N, Dong Y, Xu G, Zhang Y, Shu L, Soriano SG, Zheng H, Yu B, Xie Z: Sevoflurane acts on ubiquitination–proteasome pathway to reduce postsynaptic density 95 protein levels in young mice. Anesthesiology 2017; 127:961–75

7. Zhang MQ, Ji MH, Zhao QS, Jia M, Qiu LL, Yang JJ, Peng YG, Yang JJ, Martynyuk AE: Neurobehavioural abnormalities induced by repeated exposure of neonatal rats to sevoflurane can be aggravated by social isolation and enrichment deprivation initiated after exposure to the anaesthetic. Br J Anaesth 2015; 115:752–60

8. Dong Y, Liang F, Huang L, Fang F, Yang G, Tanzi RE, Zhang Y, Quan Q, Xie Z: The anesthetic sevoflurane induces tau trafficking from neurons to microglia. Commun Biol 2021; 4:560

9. Zhou B, Chen L, Liao P, Huang L, Chen Z, Liao D, Yang L, Wang J, Yu G, Wang L, Zhang J, Zuo Y, Liu J, Jiang R: Astroglial dysfunctions drive aberrant synaptogenesis and social behavioral deficits in mice with neonatal exposure to lengthy general anesthesia. PLoS Biol 2019; 17:e3000086

10. Wu Z, Xue H, Gao Q, Zhao P: Effects of early postnatal sevoflurane exposure on oligodendrocyte maturation and myelination in cerebral white matter of the rat. Biomed Pharmacother 2020; 131:110733

11. Song SY, Meng XW, Xia Z, Liu H, Zhang J, Chen QC, Liu HY, Ji FH, Peng K: Cognitive impairment and transcriptomic profile in hippocampus of young mice after multiple neonatal exposures to sevoflurane. Aging (Albany NY) 2019; 11:8386–417

12. Lerman J, Sikich N, Kleinman S, Yentis S: The pharmacology of sevoflurane in infants and children. Anesthesiology 1994; 80:814–24

13. Butler A, Hoffman P, Smibert P, Papalexi E, Satija R: Integrating single-cell transcriptomic data across different conditions, technologies, and species. Nat Biotechnol 2018; 36:411–20

14. Huang B, Chen Z, Geng L, Wang J, Liang H, Cao Y, Chen H, Huang W, Su M, Wang H, Xu Y, Liu Y, Lu B, Xian H, Li H, Li H, Ren L, Xie J, Ye L, Wang H, Zhao J, Chen P, Zhang L, Zhao S, Zhang T, Xu B, Che D, Si W, Gu X, Zeng L, Wang Y, Li D, Zhan Y, Delfouneso D, Lew AM, Cui J, Tang WH, Zhang Y, Gong S, Bai F, Yang M, Zhang Y: Mucosal profiling of pediatric-onset colitis and IBD reveals common pathogenics and therapeutic pathways. Cell 2019; 179:1160–76.e24

15. Ni G, Yang X, Li J, Wu X, Liu Y, Li H, Chen S, Fogarty CE, Frazer IH, Chen G, Liu X, Wang T: Intratumoral injection of caerin 1.1 and 1.9 peptides increases the efficacy of vaccinated TC-1 tumor-bearing mice with PD-1 blockade by modulating macrophage heterogeneity and the activation of CD8(+) T cells in the tumor microenvironment. Clin Transl Immunology 2021; 10:e1335

16. Habib N, Li Y, Heidenreich M, Swiech L, Avraham-Davidi I, Trombetta JJ, Hession C, Zhang F, Regev A: Div-seq: Single-nucleus RNA-seq reveals dynamics of rare adult newborn neurons. Science 2016; 353:925–8

17. Artegiani B, Lyubimova A, Muraro M, van Es JH, van Oudenaarden A, Clevers H: A single-cell RNA sequencing study reveals cellular and molecular dynamics of the hippocampal neurogenic niche. Cell Rep 2017; 21:3271–84

18. Arneson D, Zhang G, Ying Z, Zhuang Y, Byun HR, Ahn IS, Gomez-Pinilla F, Yang X: Single cell molecular alterations reveal target cells and pathways of concussive brain injury. Nat Commun 2018; 9:3894

19. Han X, Wang R, Zhou Y, Fei L, Sun H, Lai S, Saadatpour A, Zhou Z, Chen H, Ye F, Huang D, Xu Y, Huang W, Jiang M, Jiang X, Mao J, Chen Y, Lu C, Xie J, Fang Q, Wang Y, Yue R, Li T, Huang H, Orkin SH, Yuan GC, Chen M, Guo G: Mapping the mouse cell atlas by Microwell-seq. Cell 2018; 172:1091–107.e17

20. Efremova M, Vento-Tormo M, Teichmann SA, Vento-Tormo R: CellPhoneDB: inferring cell-cell communication from combined expression of multi-subunit ligand-receptor complexes. Nat Protoc 2020; 15:1484–506

21. Trapnell C, Cacchiarelli D, Grimsby J, Pokharel P, Li S, Morse M, Lennon NJ, Livak KJ, Mikkelsen TS, Rinn JL: The dynamics and regulators of cell fate decisions are revealed by pseudotemporal ordering of single cells. Nat Biotechnol 2014; 32:381–6

22. Wang J, Xu Y, Chen Z, Liang J, Lin Z, Liang H, Xu Y, Wu Q, Guo X, Nie J, Lu B, Huang B, Xian H, Wang X, Wu Q, Zeng J, Chai C, Zhang M, Lin Y, Zhang L, Zhao S, Tong Y, Zeng L, Gu X, Chen ZG, Yi S, Zhang T, Delfouneso D, Zhang Y, Nutt SL, Lew AM, Lu L, Bai F, Xia H, Wen Z, Zhang Y: Liver immune profiling reveals pathogenesis and therapeutics for biliary atresia. Cell 2020; 183:1867–83.e26

23. Finak G, McDavid A, Yajima M, Deng J, Gersuk V, Shalek AK, Slichter CK, Miller HW, McElrath MJ, Prlic M, Linsley PS, Gottardo R: MAST: A flexible statistical framework for assessing transcriptional changes and characterizing heterogeneity in single-cell RNA sequencing data. Genome Biol 2015; 16:278

24. Xu C, Liu X, Fang X, Yu L, Lau HC, Li D, Liu X, Li H, Ren J, Xu B, Jiang J, Tang L, Chen X: Single-cell RNA sequencing reveals smooth muscle cells heterogeneity in experimental aortic dissection. Front Genet 2022; 13:836593

25. Ashburner M, Ball CA, Blake JA, Botstein D, Butler H, Cherry JM, Davis AP, Dolinski K, Dwight SS, Eppig JT, Harris MA, Hill DP, Issel-Tarver L, Kasarskis A, Lewis S, Matese JC, Richardson JE, Ringwald M, Rubin GM, Sherlock G: Gene ontology: Tool for the unification of biology. The Gene Ontology Consortium. Nat Genet 2000; 25:25–9

26. Ogata H, Goto S, Sato K, Fujibuchi W, Bono H, Kanehisa M: KEGG: Kyoto Encyclopedia of Genes and Genomes. Nucleic Acids Res 1999; 27:29–34

27. Anacker C, Luna VM, Stevens GS, Millette A, Shores R, Jimenez JC, Chen B, Hen R: Hippocampal neurogenesis confers stress resilience by inhibiting the ventral dentate gyrus. Nature 2018; 559:98–102

28. Hickman S, Izzy S, Sen P, Morsett L, El Khoury J: Microglia in neurodegeneration. Nat Neurosci 2018; 21:1359–69

29. Hickman SE, Kingery ND, Ohsumi TK, Borowsky ML, Wang LC, Means TK, El Khoury J: The microglial sensome revealed by direct RNA sequencing. Nat Neurosci 2013; 16:1896–905

30. Vasek MJ, Garber C, Dorsey D, Durrant DM, Bollman B, Soung A, Yu J, Perez-Torres C, Frouin A, Wilton DK, Funk K, DeMasters BK, Jiang X, Bowen JR, Mennerick S, Robinson JK, Garbow JR, Tyler KL, Suthar MS, Schmidt RE, Stevens B, Klein RS: A complement-microglial axis drives synapse loss during virus-induced memory impairment. Nature 2016; 534:538–43

31. Zhan Y, Paolicelli RC, Sforazzini F, Weinhard L, Bolasco G, Pagani F, Vyssotski AL, Bifone A, Gozzi A, Ragozzino D, Gross CT: Deficient neuron-microglia signaling results in impaired functional brain connectivity and social behavior. Nat Neurosci 2014; 17:400–6

32. Chhor V, Le Charpentier T, Lebon S, Ore MV, Celador IL, Josserand J, Degos V, Jacotot E, Hagberg H, Savman K, Mallard C, Gressens P, Fleiss B: Characterization of phenotype markers and neuronotoxic potential of polarised primary microglia in vitro. Brain Behav Immun 2013; 32:70–85

33. Soltesz I, Losonczy A: CA1 pyramidal cell diversity enabling parallel information processing in the hippocampus. Nat Neurosci 2018; 21:484–93

34. Azim K, Angonin D, Marcy G, Pieropan F, Rivera A, Donega V, Cantu C, Williams G, Berninger B, Butt AM, Raineteau O: Pharmacogenomic identification of small molecules for lineage specific manipulation of subventricular zone germinal activity. PLoS Biol 2017; 15:e2000698

35. Bassett DS, Sporns O: Network neuroscience. Nat Neurosci 2017; 20:353–64

36. Gonçalves JT, Schafer ST, Gage FH: Adult neurogenesis in the hippocampus: From stem cells to behavior. Cell 2016; 167:897–914

37. Boldrini M, Fulmore CA, Tartt AN, Simeon LR, Pavlova I, Poposka V, Rosoklija GB, Stankov A, Arango V, Dwork AJ, Hen R, Mann JJ: Human hippocampal neurogenesis persists throughout aging. Cell Stem Cell 2018; 22:589–99.e5

38. Zrzavy T, Hametner S, Wimmer I, Butovsky O, Weiner HL, Lassmann H: Loss of "homeostatic" microglia and patterns of their activation in active multiple sclerosis. Brain 2017; 140:1900–13

39. Lawson LJ, Perry VH, Dri P, Gordon S: Heterogeneity in the distribution and morphology of microglia in the normal adult mouse brain. Neuroscience 1990; 39:151–70

40. Jimenez JC, Berry JE, Lim SC, Ong SK, Kheirbek MA, Hen R: Contextual fear memory retrieval by correlated ensembles of ventral CA1 neurons. Nat Commun 2020; 11:3492

41. Clausen NG, Hansen TG, Disma N: Anesthesia neurotoxicity in the developing brain: Basic studies relevant for neonatal or perinatal medicine. Clin Perinatol 2019; 46:647–56

42. Cohen CCH, Popovic MA, Klooster J, Weil MT, Möbius W, Nave KA, Kole MHP: Saltatory conduction along myelinated axons involves a periaxonal nanocircuit. Cell 2020; 180:311–22.e15

43. Zhang L, Xue Z, Liu Q, Liu Y Xi S, Cheng Y, Li J, Yan J, Shen Y, Xiao C, Xie Z, Qiu Z, Jiang H: Disrupted folate metabolism with anesthesia leads to myelination deficits mediated by epigenetic regulation of ERMN. EBioMedicine 2019; 43:473–86

44. Fan Z, Liang L, Ma R, Xie R, Zhao Y, Zhang M, Guo B, Zeng T, He D, Zhao X, Zhang H: Maternal sevoflurane exposure disrupts oligodendrocyte myelination of the postnatal hippocampus and induces cognitive and motor impairments in offspring. Biochem Biophys Res Commun 2022; 614:175–82

45. Glasgow SD, Wong EW, Thompson-Steckel G, Marcal N, Séguéla P, Ruthazer ES, Kennedy TE: Pre- and post-synaptic roles for DCC in memory consolidation in the adult mouse hippocampus. Mol Brain 2020; 13:56

46. Yadav R, Hillman BG, Gupta SC, Suryavanshi P, Bhatt JM, Pavuluri R, Stairs DJ, Dravid SM: Deletion of glutamate delta-1 receptor in mouse leads to enhanced working memory and deficit in fear conditioning. PLoS One 2013; 8:e60785

47. Zaslavsky K, Zhang WB, McCready FP, Rodrigues DC, Deneault E, Loo C, Zhao M, Ross PJ, El Hajjar J, Romm A, Thompson T, Piekna A, Wei W, Wang Z, Khattak S, Mufteev M, Pasceri P, Scherer SW, Salter MW, Ellis J: SHANK2 mutations associated with autism spectrum disorder cause hyperconnectivity of human neurons. Nat Neurosci 2019; 22:556–64

48. Matter C, Pribadi M, Liu X, Trachtenberg JT: Delta-catenin is required for the maintenance of neural structure and function in mature cortex in vivo. Neuron 2009; 64:320–7

49. Wang Y, Kerrisk Campbell M, Tom I, Foreman O, Hanson JE, Sheng M: PCDH7 interacts with GluN1 and regulates dendritic spine morphology and synaptic function. Sci Rep 2020; 10:10951

50. Chen Z, Montcouquiol M, Calderon R, Jenkins NA, Copeland NG, Kelley MW, Noben-Trauth K: Jxc1/Sobp, encoding a nuclear zinc finger protein, is critical for cochlear growth, cell fate, and patterning of the organ of corti. J Neurosci 2008; 28:6633–41